Doctoral Dissertation

Study on mechanoradical generation and application in azo-crosslinked double network hydrogels

（アゾ架橋ダブルネットワークゲルにおけるメカノラジカルの発生と応用に関する研究）

Zhi Jian Wang

Laboratory of Soft and Wet Matter

Division of Soft Matter

Graduate School of Life Science,

Hokkaido University, Japan

September 2022

Content

Content.....i
List of important abbreviations.....iv

Chapter 1: General Introduction 1

1.1 Overview 1

1.2 Background 3

1.2.1 Double/multiple network materials 3

1.2.2 Mechanochemistry in double/multiple network materials. 4

1.2.3 Reactivity of mechanoradicals.....5

1.3 References 6

Chapter 2: Mechanoradical generation in azo-crosslinked double network hydrogels.....10

2.1 Introduction 10

2.2 Experiments.....11

2.2.1 Materials 11

2.2.2 Synthesis of azoalkane crosslinker 12

2.2.3 Synthesis of DN gels with different crosslinkers 13

2.2.4 Length swelling ratio of the gels 13

2.2.5 Mechanical measurement of the gels.....14

2.2.6 Evaluation of mechanoradical concentration by Fenton color reaction 14

2.2.7 Repetitive loading-unloading test of DN gels fed with AMPS and TADETA 15

2.2.8 Force-responsive functionalization of DN gels fed with NIPAm and MBA 15

2.2.9 Measurement of polymer weight fraction of the gels.....15

2.2.10 Data analysis.....16

2.2.11 Computational methods.....16

2.3 Results and Discussion 17
2.3.1 Density functional theory simulation of the bond rupture under the force 17
2.3.2 Influence of azoalkane group on the mechanical properties 18
2.3.3 Influence of azoalkane group on the mechanoradical concentration 20
2.3.4 Advantage of high concentration of mechanoradicals 23
2.4 Conclusions 24
2.5 References 40
Chapter 3: Hydrogel morphogenesis induced by force-controlled growth 43
3.1 Introduction 43
3.2 Experiments 45
3.2.1 Materials 45
3.2.2 Shape retention ratio of the stretched DN gels 45
3.2.3 Measurement of polymer weight fraction of the gels 46
3.2.4 Measurement of width and modulus after different dwell time 46
3.2.5 Forming by drawing and blowing 46
3.3 Results and Discussion 47
3.3.1 Plasticity of DN gels by mechanoradical polymerization 47
3.3.2 Morphogenesis induced by force-controlled growth of DN-AAC gels 51
3.4 Conclusion 52
3.5 References 64
Chapter 4: Enhanced crack resistance of double network hydrogels via mechanoradical polymerization in the crack tip 67
4.1 Introduction 67
4.2 Experiments 69
4.2.1 Preparation of the hydrogels 69
4.2.2 Mechanical tests 70
4.2.3 Methods of dyeing 70

4.3 Results and Discussion 71
4.3.1 Uniaxial tensile test 71
4.3.2 Single edge notched test 73
4.3.3 Pure shear test and trouser tearing test 77
4.3.4 The generality of the strategy 78
4.4 Conclusion 79
4.5 References 80
Chapter 5: General Conclusion and Outlook 101
List of Publications 103
Acknowledgement 104

List of important abbreviations

SN	Single network
DN	Double network
(P)AMPS	(Poly)2-acrylamido-2-methyl-1-propanesulfonic acid
(P)AAm	(Poly)acrylamide
MBA	*N,N′*-methylenebis(acrylamide)
AAC	Azoalkane crosslinker
DN-MBA	DN gels with their first network crosslinked by MBA
DN-AAC	DN gels hydrogels with their first network crosslinked by AAC
DN-MIX	DN gels with their first network crosslinked by a 1:1 molar ratio mixture of AAC and MBA
DAC	(2-(acryloyloxy)ethyl) trimethylammonium chloride
DN-H_2O	DN gels fed without monomers and crosslinkers
DN-DAC	DN gels fed with monomer DAC and crosslinker MBA
(P)NIPAm	(Poly)*N*-isopropyl acrylamide

Chapter 1: General Introduction

1.1 Overview

The bond rupture of polymer chains induced by mechanical stress accompanies the generation of radicals at the ends of the broken polymer chains[1-7]. These generated radicals, called as mechanoradicals, are chemically reactive. They can trigger the chemical reactions to impart mechanical and functional improvement to the materials, including oxidation reaction[5] and free-radical polymerization[3,6-8]. Thus, mechanoradicals are going to be tools to design mechano-responsive materials.

A huge progress reported by our group is utilizing mechanoradicals to achieve the self-strengthening material in response to mechanical forces, similar to the skeletal muscle growth induced by physical exercise[7,8]. Generated mechanoradicals trigger the polymerization of monomers and crosslinkers present within the material, which can improve the mechanical properties of the material. The key to the success of this strategy is the use of double network (DN) hydrogels that enable permeability to small molecules and efficient mechanoradical generation. DN gels consist of two interpenetrating polymer networks with contrasting mechanical properties[9-11]. As a typical example, one is highly crosslinked brittle poly(2-acrylamido-2-methyl-1-propanesulfonic acid) (PAMPS) as the first network, the other is loosely crosslinked stretchable polyacrylamide (PAAm) as the second network. Such a contrasting structure leads to a great number of bond ruptures of the first network to generate mechanoradicals during loading, whereas the second network maintains the integrity of the gel. In comparison, the rupture of a few polymer strands in the conventional single network (SN) hydrogels will trigger the catastrophic failure of the material. Thus, mechanoradical concentration in DN gels is much higher than that in SN gels and is

able to trigger the mechanoradicals polymerization. Despite this, the mechanoradical concentration in DN gels is still relatively low, which causes the limitation of the argon atmosphere and long polymerization time. The low concentration of mechanoradicals also limits the further mechanoresponsive function development in DN gels utilizing mechanoradicals.

Thus, this doctoral dissertation devotes to increasing the mechanoradicals in DN gels and to introducing more unique properties to DN gels via mechanoradical polymerization. This dissertation comprises five chapters including this general introduction and background as **Chapter 1**.

In Chapter 2, we demonstrate that by incorporating a weak azoalkane crosslinker, instead of traditional crosslinker *N,N′*-methylenebis(acrylamide) (MBA), into the first network of DN gels, the mechanoradical concentration in stretched DN gels is much improved. We compare the difference between azo-crosslinked DN gels and MBA-crosslinked DN gels in the mechanical properties and mechanoradical generation performance. We then demonstrate that the improved mechanoradical concentration attained in azo-crosslinked DN gels can significantly accelerate the mechanoradical polymerization process. Other novel function development of DN gels based on the improved mechanoradical concentration is in Chapter 3 and Chapter 4.

In Chapter 3, we demonstrate force-controlled morphogenesis of azo-crosslinked DN gels. We explored the experiment conditions on how to use the mechanoradical triggered new network to confer plasticity to the elastic DN gel. With this plasticity, we successfully regulated the sheet-shaped double network hydrogels into various three-dimensional shapes at ambient temperature by applying existing shaping processes such as blowing and drawing.

In Chapter 4, we utilized the mechanoradicals and resultant newly formed network

in the crack tip to enhance the crack resistance of azo-crosslinked DN gels. We performed a single edge notched test, pure shear test, and tearing test to demonstrate how mechanoradical polymerization in the crack tip rate dependently improves the flaw sensitivity and influences the crack propagation. By the way, the unique two-section rate-dependent tensile behavior induced by mechanoradical polymerization is demonstrated.

In Chapter 5, conclusion remarks of this research are summarized.

1.2 Background

1.2.1 Double/multiple network materials

Since Gong et al. demonstrated that a double network hydrogel shows extremely high strength and toughness in 2003 (**Figure 1.1**), the double/multiple network (DN/MN) strategy has been gradually accepted as an effective way to toughen not only hydrogels but also elastomers[11]. The essence of this strategy is to combine a stiff and brittle first network with a soft and stretchable second network. Upon loading, the first brittle network breaks to dissipate massive energy, while the second stretchable network sustains deformation. This fracture mechanism generally accounts for the strength and toughness of DN gels when subjected to the mechanical forces. Besides, the following details related to this dissertation should be paid special attention to.

One is yielding, necking, and hysteresis[12-14]. On tensile tests of some DN gels, yielding and subsequent necking phenomenon (referring to a disproportional decrease of the cross-section area), were observed. Accordingly, the mechanical behavior of DN gels during the deformation can be divided into three zones, i.e., pre-necking, necking, and post-necking. At the pre-necking region, only a small part of relatively short chains in the first network was broken due to their limited stretchability. During the necking propagation, extensive bond rupture of the first network occurs in the necked region,

which is reflected in the hysteresis of the first loading curves. That's why the mechanoradicals are mainly generated in the necked region. Since the covalent bond rupture is irreversible, the initial stiffness inevitably drops upon the second loading. In the post-necking zone, the second network is responsible for the hardening of the gel while the broken first network has a negligible contribution to it.

Based on the necking phenomena and the large hysteresis of DN gels, Brown[15] and Tanaka[16] have independently proposed a similar model for explaining the extraordinarily high fracture energy. According to this model, a necked damage zone is formed at the crack tip. In this case, the fracture toughness, Γ, of the DN gels is not only determined by the intrinsic fracture energy Γ_0, but also contributed by the energy dissipation of rupturing the first network in the damage zone Γ_{diss}, i.e., $\Gamma = \Gamma_0 + \Gamma_{diss.}$ This damage zone was later confirmed by a direct observation via a phase contrast microscope[17] and by an indirect way via visualization of covalent bond scission through mechanoradical polymerization[8].

1.2.2 Mechanochemistry in double/multiple network materials.

The structure feature of DN/MN polymer materials makes it easy to transfer the applied external mechanical force to the polymer chains in the first network. It encourages the researchers to incorporate mechanophores into the first network of the double/multiple network polymer materials to sense the stress and design mechano-responsive materials, including force-responsive color change, luminescence, isomerization, catalyst, and small molecule release. For example, Ducrot et al.[18] incorporated the chemiluminescent cross-linking molecules, which emit light as they break, into the first network of MN elastomers. In this way, the MN elastomers can excite the luminescence in response to the external force and can be mapped in real time where and when many of these internal bonds break ahead of a propagating crack.

The author's group later[19-21] incorporated the spirogyra into the different networks of the DN/MN elastomers to reveal the stress transfer in different networks under the mechanical force. Bhakthi et al.[22] reported oxanorbornadiene cross-linked double network hydrogels that release molecules through a force-mediated retro Diels–Alder reaction. Qiu et al.[23] demonstrated that when mechanophore is incorporated in the pre-stretched first network, it can lower the activation energy of mechanophores.

1.2.3 Reactivity of mechanoradicals

Exerting the mechanical force into the polymer materials causes the bond rupture of polymer chains, which accompanies the generation of radicals at the end of the broken chains. It is directly confirmed by using electron paramagnetic resonance[4]. Generated radicals are reactive to participating the chemical reactions. To my best knowledge, it is first reported in 1956 that the softening of rubbers on mastication is a consequence of scission of the rubber molecules by the applied shear. Generated radicals were utilized to initiate the polymerization of the monomers present in the rubber[2-4]. Then Baytekin et al.[5] found that mechanoradicals can react with water the generate hydrogen peroxide and can induce the deposition of metal nanoparticles from metal salts in a solution. More recently, Kubota et al.[24] reported polymeric mechanoradicals were formed in situ under ball-milling conditions, which can undergo radical–radical coupling with a pre-fluorescent nitroxide-based reagent to generate a fluorescent polymer. We believe radicals generated at the ends of the polymer chains induced by the external force can work similarly to the thermo- or light-initiated radicals. Of course, the mobility of macro-mechanoradicals should be lower than normal small radicals.

1.3 References

1. Meville, H. W., Murray, J. R. The ultrasonic degradation of polymers. *Trans. Faraday Soc.* **1950**, *46*, 996-1009.
2. Ayrey, G., Moore, C. G., Watson, W. F. Mastication. Part III. Chemical verification of the mechanical degradation mechanism of cold mastication. *J. Polym. Sci.* **1956**, 19, 1-15.
3. Angier, D. J., Watson, W. F. Mastication of rubber. IV. Polymerization of vinyl monomers by the cold mastication of rubber. *Rubber Chem. Tech.* **1956**, *29*, 1140-1153.
4. Sohma, J. Mechanochemistry of polymers. *Pro. Polym. Sci.* **1989**, *14*, 451-596.
5. Baytekin, H. T.; Baytekin, B.; Grzybowski, B. A. Mechanoradicals created in "polymeric sponges" drive reactions in aqueous media. *Angew. Chem., Int. Ed. Engl.* **2012**, *51*, 3596−3600.
6. Sakaguchi, M., Sohma, J. Copolymerizations initiated by mechano-radicals on particle surfaces of poly (tetrafluoroethylene). *J. Appl. Polym. Sci.* **1978**, *22*, 2915-2924.
7. Matusda, T., Kawakami, R., Namba, R., Nakajima, T., Gong, J. P. Mechanoresponsive self-growing hydrogels inspired by muscle training. *Science* **2019**, *363*, 504-508.
8. Matsuda, T.; Kawakami, R.; Nakajima, T.; Gong, J. P. Crack tip field of a double-network gel: visualization of covalent bond scission through mechanoradical polymerization. *Macromolecules* **2020**, *53*, 8787−8795.
9. Gong, J. P.; Katsuyama, Y.; Kurokawa, T.; Osada, Y. Double network hydrogels with extremely high mechanical strength. *Adv. Mater.* **2003**, *15*, 1155−1158.
10. Gong, J. P. Why are double network hydrogels so tough? *Soft Matter* **2010**, *6*,

2583−2590.

11. Yang, J., Li, K., Tang, C., Liu, Z., Fan, J., Qin, G., Cui, W., Zhu, L., Chen, Q. Recent progress in double network elastomers: one plus one is greater than two. *Adv. Funct. Mater.* **2022**, *32*, 2110244.
12. Na, Y.-H.; Tanaka, Y.; Kawauchi, Y.; Furukawa, H.; Sumiyoshi, T.; Gong, J. P.; Osada, Y. Necking phenomenon of double-network gels. *Macromolecules* **2006**, *39*, 4641−4645.
13. Nakajima, T.; Kurokawa, T.; Ahmed, S.; Wu, W. l.; Gong, J. P. Characterization of internal fracture process of double network hydrogels under uniaxial elongation. *Soft Matter* **2013**, *9*, 1955−1966.
14. Morovati, V., Saadat, M. A., Dargazany, R. Necking of double-network gels: constitutive modeling with microstructural insight. *Phys. Rev. E* **2020**, *102*, 062501.
15. Brown, H. R. A model of the fracture of double network gels. *Macromolecules* **2007**, *40*, 3815-3818.
16. Tanaka, Y. A local damage model for anomalous high toughness of double network gels. *Europhys. Lett.* **2007**, *78*, 56005.
17. Liang, S., Wu, Z. L., Hu, J., Kurokawa, T., Yu, Q. M., Gong, J. P. Direct observation on the surface fracture of ultrathin film double-network hydrogels. *Macromolecules* **2011**, *44*, 3016-3020.
18. Ducrot, E., Chen, Y., Bulters, M., Sijbesma, R. P., Creton, C. Toughening elastomers with sacrificial bonds and watching them break. *Science* **2014**, *344*, 186-189.
19. Chen, Y. J.; Yeh, C. J.; Qi, Y.; Long, R.; Creton, C. From Force-responsive molecules to quantifying and mapping stresses in soft materials. *Sci. Adv.* **2020**, *6*, eaaz5093.

20. Chen, Y. J.; Yeh, C. J.; Guo, Q.; Qi, Y.; Long, R.; Creton, C. Fast reversible isomerization of merocyanine as a tool to quantify stress history in elastomers. *Chem. Sci.* **2020**, *12*, 1693−1701.
21. Chen, Y.; Sanoja, G.; Creton, C. Mechanochemistry unveils stress transfer during sacrificial bond Fracture of tough multiple network elastomers. *Chem. Sci.* **2021**, *12*, 11098−11108.
22. Jayathilaka, P. B., Molley, T. G., Huang, Y., Islam, M. S., Buche, M. R., Silberstein, M. N., Kruzic, J. J., Kilian, K. A. Force-mediated molecule release from double network hydrogels. *Chem. Comms.* **2021**, *57*, 8484-8487.
23. Qiu, W.; Gurr, P. A.; Qiao, G. G. Regulating color activation energy of mechanophore-linked multinetwork elastomers. *Macromolecules* **2020**, *53*, 4090-4098.
24. Kubota, K., Toyoshima, N., Miura, D., Jiang, J., Maeda, S., Jin, M., Ito, H. Introduction of a luminophore into generic polymers via mechanoradical coupling with a prefluorescent reagent. *Angew. Chem*. **2021**, *133*, 16139-16144.

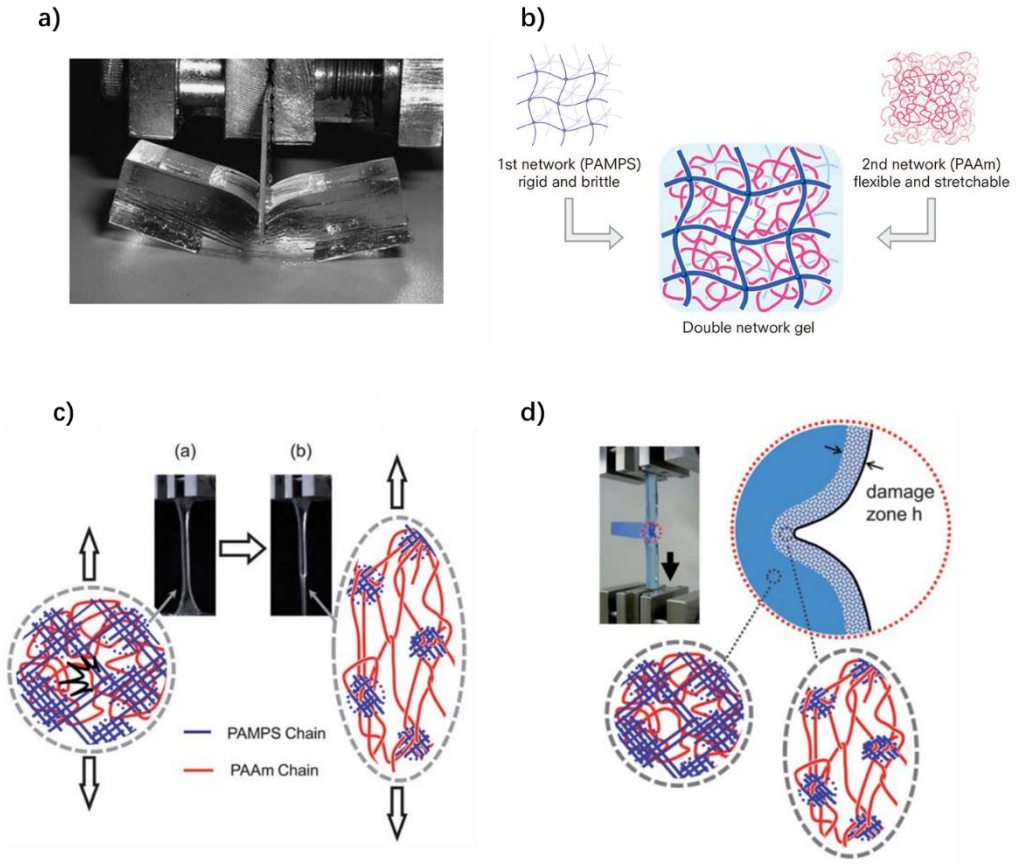

Figure 1.1. a) Demonstration showing extremely toughness of double network hydrogels. b) Illustration of the network structure of a classic DN hydrogels. c) Illustration showing the necking phenomenon and internal structure change in the necked region. d) Illustration of the local damage zone at the crack front of DN gels. Panels (a,c,d) are reproduced with permission. Copyright 2010, Royal Society Chemistry.

Chapter 2: Mechanoradical generation in azo-crosslinked double network hydrogels

2.1 Introduction

As described in Chapter 1, a further increase in the concentration of mechanoradicals generated in DN gels will provide added benefits, such as relaxation in the requirements for an anaerobic environment for polymerization, and an increase in the reaction rate, thereby widening the application fields of mechanoradicals.

The generation of mechanoradicals derives from the bond rupture of the brittle PAMPS network. To increase the mechanoradical concentration is to increase the number of bond ruptures of the first network when DN gels are subjected to the external forces. The first network of the conventional DN gels is composed of the main chains of carbon−carbon (C-C) bonds and the crosslinking points containing amide bonds (C-N). These bonds are strong bonds with a high bond dissociation energy (BDE, ~ 250 – 400 kJ/mol)[1,2]. Considering this, incorporating weak bonds with a lower bond dissociation energy into the main chain or crosslinking point in the first network should be a good idea to induce more bond rupture.

Actually, incorporating weak covalent bonds in polymer materials is a widely used strategy for designing mechanosensitive materials[3-15]. When embedded in polymeric materials, they can undergo site-specific bond scissions or chemical transformations in response to mechanical forces. These weak bonds include scissile bonds that break into two parts such as the peroxide bond[3,4], disulfide group[5,6], and azoalkane group[7-9] and non-scissile bonds that just change their conformation and still retain their integrity, such as the azobenzene group[10,11] and the spirogyra group[12-15]. Researchers have introduced suitable weak covalent bonds into the polymer backbone to realize the required mechanoresponsive functions.

Among these weak bonds, we focused on azoalkane (R−N=N−R; BDE ~ 80−160 kJ/mol), whose azo group is connected to saturated carbon atoms, as an efficient mechanoradical source[16]. Azoalkane is one of the most widely used weak covalent bonds as initiators for radical polymerization. Azoalkane undergoes homolysis cleavage and forms reactive radicals to trigger the polymerization when exposed to heat and light. In addition, azoalkane also exhibits site-specific bond cleavage when subjected to mechanical forces[7-9].

Hence, in an attempt to induce more bond rupture in the first network and resultant more mechanoradical generation in DN gels under a mechanical force, an azoalkane-containing crosslinker (AAC) is adopted for the first PMAPS network, instead of conventional crosslinkers *N,N′*-methylenebis(acrylamide) (MBA) (**Figure 2.1a, b**).

In this chapter, we systematically investigated the effect of the AAC on the mechanical properties of the gel and bond rupture process during loading. Thus, three types of DN gels were synthesized following the conventional two-step sequential polymerization process, as shown in **Figure 2.1c**: A traditional DN-MBA gel, in which the first PAMPS network is crosslinked by the conventional crosslinker N,N'-methylenebis(acrylamide) (MBA); a DN-AAC gel, in which the first PAMPS network is crosslinked by an azoalkane crosslinker; and a DN-MIX gel, in which a 1:1 molar ratio mixture of MBA and AAC crosslinks the first PAMPS network. Details about gel synthesis are shown in **section 2.2.3.**

2.2 Experiments

2.2.1 Materials

Azoalkane crosslinker, 2,2’-azobis-[2-methyl-N-(2-ethylpropenoate)]-propionamide] (AAC), was prepared by treatment of 2,2'-azobis[2-methyl-N-(2-hydroxyethyl) propionamide] (VA-086) and acryloyl chloride **(Figure 2.2**). Synthesis details are

shown in **section 2.2.2.** 2-acrylamido-2-methyl-1-propanesulfonic acid (AMPS) was provided by Toagosei. Acrylamide (AAm) was purchased from Junsei Chemical. *N*,*N*'-methylenebis (acrylamide) (MBA), N,N',N''-triacryloyl diethylenetriamine (TADETA), 2,2'-azobis(2,4-dimethyl) valeronitrile (ABVN), 2,2'-azobis[2-(2-imidazolin-2-yl)propane] dihydrochloride (VA-044), *N*-isopropyl acrylamide (NIPAm), ammonium iron(II) sulfate ($(NH_4)2Fe^{II}(SO_4)_2$) hexahydrate, sulfuric acid (H_2SO_4), ammonium iron(III) sulfate ($NH_4Fe^{III}(SO4)_2$) dodecahydrate, xylenol orange (XO) were purchased from Wako Pure Chemical Industries. All reagents were used as received.

2.2.2 Synthesis of azoalkane crosslinker

To a 100 mL three-necked round-bottomed flask equipped with a magnetic stirrer and rubber stopper and purged with Argon gas were added 2,2'-azobis[2-methyl-N-(2-hydroxyethyl) propionamide] (VA-086, 1 equiv.) and CH_2Cl_2 (5 mL/mmol VA-086). The resulting suspension was cooled in a liquid nitrogen/acetone bath, then added was triethylamine (16 equiv.). After that, a solution of acryloyl chloride (6 equiv.) in CH_2Cl_2 (1 mL/mmol) was added dropwise into the suspension. The reaction mixture was stirred for 5 hours, and it was allowed to warm slowly to room temperature, then poured onto saturated $NaHCO_3$ to quench the reaction and CH_2Cl_2 to extract the organic compound. The layers were separated, and the aqueous layer was extracted with CH_2Cl_2 twice. The combined organics was washed with saturated $NaHCO_3$ then dried over Na_2SO_4. After removal of solvent by evaporation, the crude product was then purified by silica gel chromatography eluted with Hexane: EtOAc = 1: 1 and EtOAc in turn to give product as white or light-yellow solid. ^{1}H NMR (DMSO 500 MHz) δ 7.68 (2H, s) 6.30 (2H, d) 6.13 (2H, q) 5.94 (2H, d) 4.15 (4H, t) 3.44 (4H, t) 1.26 (12H, s) ^{13}C NMR (DMSO 500 MHz) δ 173.8, 165.8, 131.3, 127.7, 74.5, 62.9, 38.5, 22.7. FTMS-ESI (m/z): $[M - H]^-$

calculated for $C_{18}H_{28}N_4O_6$, 396.20; found, 396.19.

2.2.3 Synthesis of DN gels with different crosslinkers

DN hydrogels with different crosslinkers were prepared by the conventional two-step procedure. Since azoalkane group is also sensitive to high temperature and UV light, low-temperature radical polymerization was adopted to avoid decomposition of the azoalkane group in AAC during the hydrogel preparation. Thermal decomposition of the AAC during the polymerizations was found to be negligible (**Figure 2.3**).

After being bubbled with argon gas for 15 minutes, the precursor *N*,*N*-dimethylformamide solution containing AMPS (1 mol/L, monomer), 2,2'-azobis(2,4-dimethyl) valeronitrile (1% mol/L, initiator, 10-hour half-life temperature: 45 ℃) and different crosslinkers (MBA of 4-8 mol%, AAC of 4-12 mol% or MIX of 4-10 mol% in relative to monomer) was injected into the mold with two parallel glass plants and silicone spacers. Then the mold was kept at 44℃ for 10 hours to form PAMPS single network (SN) hydrogel. The resulting PAMPS SN hydrogel was then immersed into aqueous solution containing AAM (2 mol/L, monomer), MBA (0.02% mol/L, crosslinker), 2,2'-azobis[2-(2-imidazolin-2-yl)propane] dihydrochloride (0.1% mol/L, initiator, 10-hour half-life temperature: 44 ℃) for 1 day until equilibrium was reached. The equilibrated PAMPS SN hydrogel was sandwiched by two glass substrates and then kept at 44℃ for 10 hours to form DN hydrogels. The as-prepared DN gel was then swelled in a large amount of water to remove the residual and to reach the equilibrium state.

2.2.4 Length swelling ratio of the gels

The length swelling ratio of the PAMPS SN gels in the AAm monomer solution, λ_{s1}, is determined by the thickness of the equilibrated PAMPS SN gels in AAm monomer

solution divided by the thickness of the as-prepared PAMPS SN gels.

The length swelling ratio of the DN gels in the water, λ_s, is determined by the thickness of the equilibrated DN gels in water divided by the thickness of the as-prepared PAMPS SN gels.

2.2.5 Mechanical measurement of the gels

The mechanical properties of single network PAMPS gels and double network gels were investigated by the uniaxial tensile test using a universal testing machine (RTC-1150A, Orientec Co.). The tensile velocity is 100 mm/min. The Young's modulus was determined as the slope of stress−strain curves between the strain range of 0.03−0.1. The yield strain and yield stress were determined at the zero-slope point of the stress−strain curves or determined by the tangential lines method. Cyclic tensile tests were performed to obtain the dissipated energy, which was calculated by the area between the loading curve and unloading curve up to the preset tensile strain $\varepsilon_{max} = 4$.

2.2.6 Evaluation of mechanoradical concentration by Fenton color reaction

Mechanoradical concentration is investigated by the Fenton color reaction, as shown in **Figure 2.4**. DN gels with different crosslinkers were cut into dumbbell-shaped strips (17 mm gauge length and 4 mm width). The cut gels were immersed in an aqueous solution of 500 μM $(NH4)_2Fe^{II}(SO_4)_2$, 500 μM XO and 20 mM H_2SO_4 for 1 day. Then gels were stretched to the preset strain ($\varepsilon_{max} = 4$) at a velocity of 100 mm/min and then immediately recovered to the initial position, during which the stress-strain curves were recorded. After 30 mins, when no further color change was observed, the gels were cut with scissors to obtain the gel in the necked region (**Figure 2.4b**), which were used to test UV-Visible absorption spectroscopy (UV-1800, Shimadzu Co.). To quantify the Fe^{3+} concentration, a calibration experiment was done by immersing DN gels into an

aqueous solution of 0-400 μM $NH_4Fe^{III}(SO_4)_2$ (as a Fe^{3+} source), 500 μM $(NH_4)_2Fe^{II}(SO_4)_2$, 500 μM XO and 20 mM H_2SO_4 to get the calibration curve of normalized absorbance at 580 nm as a function of Fe^{3+} (**Figure 2.4c,d**). By comparing the normalized absorbance at 580 nm of DN gels after stretching with the calibration curve, we can evaluate the Fe^{3+} concentration, which is assumed to be equal to the mechanoradical concentration.

2.2.7 Repetitive loading-unloading test of DN gels fed with AMPS and TADETA

DN gels crosslinked by 10 mol% AAC, named as DN-10AAC, and DN gels crosslinked by 7 mol% MBA, named as DN-7MBA, were immersed in an aqueous solution of 0.6 M AMPS and 0.3 M TADETA for one day. Then the samples of ~1.5 mm-thick were cut into dumbbell-shaped strips (12 mm gauge length and 2 mm width). After that, dumbbell shaped DN gels in the solution were put into an argon glove box for 2 hours to remove oxygen. Then the gels were conducted cyclic tensile test with the preset strain of 4 at a velocity of 300 mm/min. After 3 minutes, the gels were conducted second cyclic tensile test at the same conditions.

2.2.8 Force-responsive functionalization of DN gels fed with NIPAm and MBA

DN-10AAC, DN-7MBA gels of ~1.5 mm-thick were cut into sheets with the size of 50 mm × 50 mm. Then the samples were immersed in an aqueous solution of 2.0 M NIPAm and 0.15 M MBA for one day. Next, the samples in the solution were placed in an argon glove box for 2 hours to remove oxygen. Then the gels were compressed by a polyacrylic resin stamp with the raised bear toe pattern. The height of the raised pattern was 2.0 mm. The compression strain was controlled at 0.8.

2.2.9 Measurement of polymer weight fraction of the gels

The polymer weight fraction of the gel (f_p) is the ratio of the polymer weight in the

gel to the total weight of the equilibrium-swollen gel. Here, we use commercial moisture meter (Moisture balance, MOC-120H) to measure the water weight fraction of the gel f_w, then to obtain f_p using the following equation f_p = 1- fw. Before measurement, treated DN gels with monomers were immersed in a large amount of deionized water to remove the residual monomers and to reach their equilibrate state. Virgin DN gels are also immersed in a large amount of water to reach their equilibrated state.

2.2.10 Data analysis

Each data point was the average of at least three measurements, and the error bars represented their standard deviations.

2.2.11 Computational methods

To understand how the external force promotes the rupture of PAMPS network, we asked Professor Satoshi Maeda and Assistant professor Julong Jiang to conduct the density functional theory simulation. They first construct a PAMPS network fragment that consists of four AMPS units (-CH_2SO_3Na group is simplified to -CH_3 to reduce computational cost) and one AAC or one MBA unit (Fig. 2a and 2b) for our theoretical study. The simulation of the tensile force used to break the covalent bond is realized by their Artificial Force Induced Reaction (AFIR) method.[17,18] The AFIR method explicitly adds an artificial force between the certain fragments of a molecule to trigger a reaction. The force is applied to the system by the following AFIR function:

$$F^{AFIR}(\mathbf{Q}) = E(\mathbf{Q}) + \rho\alpha\frac{\sum_{i\in A}\sum_{j\in B}\omega_{ij}r_{ij}}{\sum_{i\in A}\sum_{j\in B}\omega_{ij}} \quad (1)$$

In Eq. (1), $E(\mathbf{Q})$ is the original Born-Oppenheimer potential energy surface of the given geometrical parameter $\mathbf{Q}$ and the second term applies the force to the system of interest. The parameter α, controls the strength of the force added to the designated

fragments inside the molecule of interest. The force term is given as a weighted sum of the distances r_{ij} between atom i in the fragment A and atom j in the fragment B through weight function ω_{ij}. Normally, an artificial attractive force (i.e., ρ = +1 in Eq. (1)) is applied to suppress the potentially reactive atoms into a certain short distance so that a reaction can proceed. In this case, a repulsive force (realized by setting ρ to -1) is added to the two terminal CH_2 groups of the polymer fragment. Such a repulsive force therefore acts as an external tensile force that stretches the polymer chain, which models what a polymer chain experiences in the single-molecule force spectroscopy experiment. With this diagonally-added artificial force, both the PAMPS chain and the MBA molecule can experience the same level of force at the same time, therefore allowing us to explore all the possible cleavage sites in the polymer network. The above-mentioned AFIR function can be used to construct the force modified potential energy surface (FMPES). Our efforts were subsequently made to locate the transition state (TS) of the bond homolysis process for both PAMPS-MBA and PAMPS-AAC networks on such an FMPES. Once the TS structure on the FMPES is successfully optimized, the Gibbs energy barrier for the formation of mechanoradicals under that certain level of force can be realized. With the varying force level (F), we can eventually characterize how the Gibbs energy barrier ($\Delta G^{\ddagger}$) changes accordingly. With this $\Delta G^{\ddagger}$-F relationship acquired from TS optimization, the rupture force can be determined at a given time.

2.3 Results and Discussion

2.3.1 Density functional theory simulation of the bond rupture under the force

Prior to the demonstration of the experiment results, we would like to show the DFT simulation results. As shown in **Figure 2.5a, b**, there are two possible rupture sites in PAMPS-MBA network, either at C_6-C_{25} or C_{28}-C_{119} position, while there is only one

rupture site at the C-(N=N) position for PAMPS-AAC network. Their transition state calculations reveals that the Gibbs energy barrier for the rupture of PAMPS-MBA at C_6-C_{25} site or C_{28}-C_{119} site is much higher than that of PAMPS-AAC network at C-(N=N) position. Given a certain timescale (e.g., 11.6 s ~ 1.44 min, which corresponds to a barrier of 80 ~ 85 kJ/mol under room temperature according to the Eyring equation), the rupture force of PAMPS-MBA network is 3110 ~ 3210 pN at C_6-C_{25} position while that of the PAMPS-AAC network is only 1520 ~ 1670 pN (**Figure 2.5c**). These calculation results strongly suggest that a large number of mechanoradicals can be effectively generated through PAMPS-AAC network.

2.3.2 Influence of azoalkane group on the mechanical properties

We first compare the structure of the PAMPS single network (SN) hydrogels formed by different crosslinkers from their modulus and swelling ability. We vary the crosslinker concentration in feed during the first step of the polymerization of AMPS (C_{1st}, mol% in relative to AMPS monomer), whereas the second network is prepared using the same formulation for all three sets of DN gels. **Figure 2.6a** shows the Young's modulus of the as-prepared PAMPS SN gels ($E_{as\text{-}prep,1st}$) obtained using different crosslinkers. According to the phantom network model for a network with four-branched crosslinking points,[19] the number density of elastically effective polymer strands of the as-prepared PAMPS network (ν_{1st}) is proportional to its Young's modulus through the relation $\nu_{1st} = 2E_{as\text{-}prep,1st} / 3RT$, where R and T are the gas constant and absolute temperature, respectively. At the same C_{1st}, PAMPS SN gels crosslinked by AAC have a smaller Young's modulus than those crosslinked by MBA, indicating a lower ν_{1st} of the PAMPS SN gel when crosslinked by AAC. The PAMPS-MIX SN gels have almost the same $E_{as\text{-}prep,1st}$ with PAMPS-AAC at the same C_{1st}, indicating the same crosslinking density of these two sets of gels. Nevertheless, the PAMPS-AAC SN gels

show larger swelling than PAMPS-MIX when immersed in the AAm monomer solution (**Figure 2.6b**), leading to a higher length swelling ratio (λ_s) of the PAMPS-AAC network in the final equilibrated state compared with that of DN-MIX (**Figure 2.6c**). This indicates that the MBA crosslinker has a less swelling ability in water than AAC. Accordingly, the lower λ_s of DN-MBA, as depicted in **Figure 2.6c**, should be attributed to the higher crosslinking density of the MBA crosslinker and the lower swelling ability.

The mechanical performance of DN gels with different first network crosslinker varieties and concentrations is investigated using uniaxial tensile tests. As shown in **Figure 2.7**, three sets of DN gels show the same trend—the modulus (E, **Figure 2.8a**), the yield stress (σ_y, **Figure 2.8b**), and fracture stress (σ_f, **Figure 2.8c**) increase substantially with an increase in C_{1st}. On the other hand, the yield strain (ε_y, **Figure 2.8d**) depends weakly on C_{1st}, and the fracture strain (ε_f, see **Figure 2.8e**) tends to decrease with an increase in C_{1st}. This dependence on the crosslinker concentration is consistent with our previous work[20,21].

In order to compare the effect of crosslinkers on the internal fracture of the first network, we first discuss the yield point of these DN gels since yield point is characteristic to the stretching limit of the first network.[22] In all three sets of samples, yielding is observed at strains between 1.2 and 1.6. ε_y at the same C_{1st} shows less dependence on the crosslinker species. In contrast, σ_y is strongly affected by the crosslinker species. For the DN-MBA gels, σ_y increases from 0.07 MPa to 0.74 MPa when C_{1st} is increased from 4 mol% to 8 mol%, which is much higher than σ_y of DN-AAC gels (0.01 MPa - 0.15 MPa) at the same C_{1st}. Even when the C_{1st} of AAC is increased to 12 mol%, at which the DN-AAC gel breaks just after reaching the yield point, σ_y is only 0.57 MPa, still much lower than the σ_y of the DN-MBA gel with a C_{1st} of 8 mol%.

To further quantitatively study the influence of the weak azoalkane group in the PAMPS network, we need to normalize the network density and prestretch level of the PAMPS network in the three systems. We take the as-prepared PAMPS single network (SN) gels as the reference state. Based on the swelling ratio in length, we can obtain the normalized yield stress ($\sigma_y\lambda_s^2$) and yield stretch ratio ($(\varepsilon_y+1)\lambda_s$) to their respective reference states for the three sets of DN gels. **Figure 2.9a** shows the normalized yield stretch ratio $(\varepsilon_y+1)\lambda_s$ replotted as a function of ν_{1st}. At the same ν_{1st}, especially at a low ν_{1st}, the $(\varepsilon_y+1)\lambda_s$ of the DN-AAC gels is larger than that of the DN-MBA gels, indicating the better stretchability of the PAMPS network when crosslinked by AAC. For normalized yield stress $\sigma_y\lambda_s^2$, it should be proportional to the area density ($\nu_{1st}^{2/3}$) of the PAMPS network strands at the reference state times bond breaking force per strand (F)[21]:

$$\sigma_y\lambda_s^2 \propto \nu_{1st}^{2/3} \times F \qquad (2)$$

As shown in **Figure 2.9b**, the $\sigma_y\lambda_s^2$ of the three sets of DN gels increase almost linearly with $\nu_{1st}^{2/3}$, confirming the relationship of (2). The slope of the linear regression line of DN-AAC is approximately 30% smaller than that of DN-MBA. This result is reasonably in consistent with DFT calculation, clearly demonstrating that the bond breaking force of the PAMPS network crosslinked by AAC is lower than that of the network crosslinked by MBA. As for the DN-MIX gels, they show the mechanical properties closer to DN-MBA.

2.3.3 Influence of azoalkane group on the mechanoradical concentration

The mechanoradical concentration of three sets of DN gels are investigated by the Fenton color reaction (**Figure 2.4**). As shown in **Figure 2.10,** mechanoradicals only generated in the necked region, suggested by the color change in the necked region. The comparison of mechanoradical concentration in three sets of DN gels are shown in

Figure 2.11. All three types of DN gels show an increase in C_{rad} with an increase in C_{1st}. As the DN-MBA gels become brittle at C_{1st} above 7 mol% while DN-AAC gels show necking until 10 mol%, the DN gel crosslinked with 10 mol% AAC exhibits the highest C_{rad} of ~220 μM among all DN gels, which is five times the highest C_{rad} generated by the DN-MBA system. Thus, our initial aim to generate a higher concentration of mechanoradicals is realized by introducing AAC crosslinks. Interestingly, the dominant species to generate radicals are not always DN-AAC gels. At the C_{1st} values of 6 mol% and 7 mol%, the DN-MIX gels are capable of generating more radicals than the other two sets of DN gels. And at C_{1st} values of 8 mol% and 9 mol%, the C_{rad} of DN-MIX is almost equal to that of the DN-AAC gels. These results show that the use of a mixture of MBA and AAC crosslinkers in the synthesis of DN gels can also generate a high C_{rad}, which is beneficial for reducing the amount of AAC used.

As analyzed previously, the mechanoradicals are generated from the bond rupture of the first network strands. Thus, the C_{rad} is proportional to the PAMPS network density at swelling equilibrated state ($\nu_{equ,1st} = \nu_{1st} / \lambda_s^3$) at which the mechanical deformation was performed. As shown in **Figure 2.12a**, $\nu_{equ,1st}$ increases with C_{1st} for all three DN gels and $\nu_{equ,1st}$ of DN-MBA is larger than that of DN-AAC and DN-MBA at the same C_{1st}. As depicted in **Figure 2.12b**, for the same $\nu_{equ,1st}$, C_{rad} of DN-AAC and DN-MIX is larger than that of DN-MBA, especially at high $\nu_{equ,1st}$. This result indicates that a larger fraction of the first network strands is ruptured when crosslinked by AAC or AAC-MBA mixture. To analyze the fraction of strand ruptured at varied crosslinking density, we express the C_{rad} as the product of the PAMPS network density ($\nu_{equ,1st}$) and the ratio of broken strands to total strands of the PAMPS network (φ_b):

$$C_{rad} = 2\, \nu_{equ,1st} \times \varphi_b \qquad (3)$$

The prefactor 2 in Equation (3) is because one bond cleavage generates two radicals.

The φ_b estimated from Equation (3) exhibited very different behaviors against C_{1st} and $\nu_{equ,1st}$ for the three sets of DN gels (**Figure 2.12c,d**). φ_b of DN-MBA monotonously decreases with increase of C_{1st} and $\nu_{equ,1st}$, whereas φ_b of DN-AAC and DN-MIX shows maximum at certain C_{1st} and $\nu_{equ,1st}$. More importantly, DN-AAC and DN-MIX show much larger φ_b than that of DN-MBA when the C_{1st} or $\nu_{equ,1st}$ is not too low, resulting from the labile azoalkane group under the external force. The trend of φ_b gives an insight of the rupture efficiency of these DN gels. To achieve a high concentration of mechanoradicals in the stretched gels, high values for $\nu_{equ,1st}$ and φ_b are both required. The lower $\nu_{equ,1st}$ of DN-AAC at C_{1st} from 4 mol% to 7 mol% results in a lower C_{rad} than DN-MBA or DN-MIX at the same C_{1st}.

Next, we investigate the energy efficiency for radical generation in the three sets of DN gels, characterized by the ratio of C_{rad} to the dissipated energy U_{hys}. Assuming that U_{hys} is entirely consumed in the bond scissions of the first network strands, the following relation between C_{rad} and U_{hys} is obtained by applying the classical Lake-Thomas theory:[23,24]

$$C_{rad} \propto 2\, U_{hys} / N U_b \qquad (4)$$

where U_b represents the dissociation energy of a single bond, and N is the monomer segment number of a strand between crosslinking points. Because the monomer concentration of the first network at preparation is the same, N is inversely proportional to ν_{1st}, assuming that all monomers are incorporated into the elastically effective strands of the network. Thus, the relation (4) can be rewritten as:

$$C_{rad} / U_{hys} \propto 2 / N U_{b,} \propto 2\, \nu_{1st} / U_b \qquad (5)$$

Equation (5) predicts a higher energy efficiency for radical generation in DN-AAC gels than DN-MBA gels, as the U_b of AAC bond is much lower. As shown in **Figure 2.13**, at the same ν_{1st}, the C_{rad}/U_{hys} of DN-AAC is approximately ten times that of DN-MBA.

This is much higher than that predicted from their difference in U_b by Equation (5). The C_{rad}/U_{hys} of DN-MIX is between those of DN-AAC and DN-MBA but much closer to that of DN-AAC gels, demonstrating that the bond scissions in the DN-MIX gel are dominated by the weak azoalkane group. These analyses confirm the feasibility of our strategy to increase the mechanoradical concentration by incorporating a weak azoalkane group into the system.

2.3.4 Advantage of high concentration of mechanoradicals

The substantially high mechanoradical concentration attained in DN gels still cannot completely eliminate the limitation of an oxygen-free environment; however, the limit to the maximum allowable dissolved oxygen in water for mechanoradical polymerization is increased, and the mechanoradical polymerization process is accelerated. To demonstrate this effect, we choose a DN-10AAC gel and a DN-7MBA gel that have the similar mechanical behaviors in their virgin state for comparison. Here the numbers 10 in 10AAC and 7 in 7MBA represent the corresponding C_{1st} values. First, we compare the force-responsive performances of two DN gels by their appearance change. After 2 h of deaeration in an argon glove box, the two DN gels fed with *N*-isopropylacrylamide (NIPAM, 2.0 M) and the MBA crosslinker (0.15 M) are compressed by a stamp with a raised bear toe shape (**Figure 2.14a**). After 3 min, the DN-10AAC gel directly show a distinct bear toe pattern at the ambient temperature, resulting from the formation of a highly crosslinked PNIPAm network in the compressed region (**Figure 2.14b**). This is further confirmed by the fact that the polymer weight fraction in the compressed region increases from 12% to 19% (**Figure 2.15a**). In comparison, the DN-7MBA gel shows no distinct change in appearance even after 30 min and no increase in the polymer weight fraction, indicating that polymerization hardly occurs under the same deaeration conditions. Then we

demonstrate that substantially high concentration of mechanoradicals in DN-10AAC can also be used to realize a fast stretching-triggered mechanical growth of the gels. These two DN gels are fed with monomer AMPS (0.6 M) and crosslinker *N*,*N*',*N*''-triacryloyl diethylenetriamine (TADETA; 0.3 M) and are performed with cyclic loading-unloading tests twice with an interval of 3 min (**Figure 2.14c**) in the argon glove box. In contrast to the DN-7MBA gel, which shows mechanical hysteresis only in the first cycle, the DN-10AAC gel shows hysteresis and the force increase in the second cycle (**Figure 2.14d**). Specifically, to the same gauge length of 50 mm, the retraction force of DN-10AAC is 0.8 N at the first loading but decreases to 0.2 N at the first unloading due to the permanent rupture of the brittle network. However, at the second loading it increases to the larger value of 1.0 N. The force enhancement indicates the rapid formation of a new network in the DN-10AAC gel after the first stretching cycle due to highly efficient mechanoradical generation. In fact, the polymer weight fraction in the stretched region of DN-10AAC increases from 12% to 23%, but not in the DN-7MBA gel (**Figure 2.15b**).

2.4 Conclusions

In summary, we have incorporated the azoalkane crosslinker AAC into the first PAMPS network in DN gels and demonstrate that the incorporation of AAC remarkably increases the mechanoradical concentration compared to the commercial crosslinker MBA. The energy efficiency for mechanoradical generation is also much improved by using AAC crosslinker. Employing a mixture of MBA and AAC crosslinkers results in a comparable crosslinking efficiency as MBA alone but an excellent performance in generating mechanoradicals as like AAC alone. The increased mechanoradical concentration accelerates force-triggered polymerization and is beneficial for extending the application of DN gels in force-responsive fields.

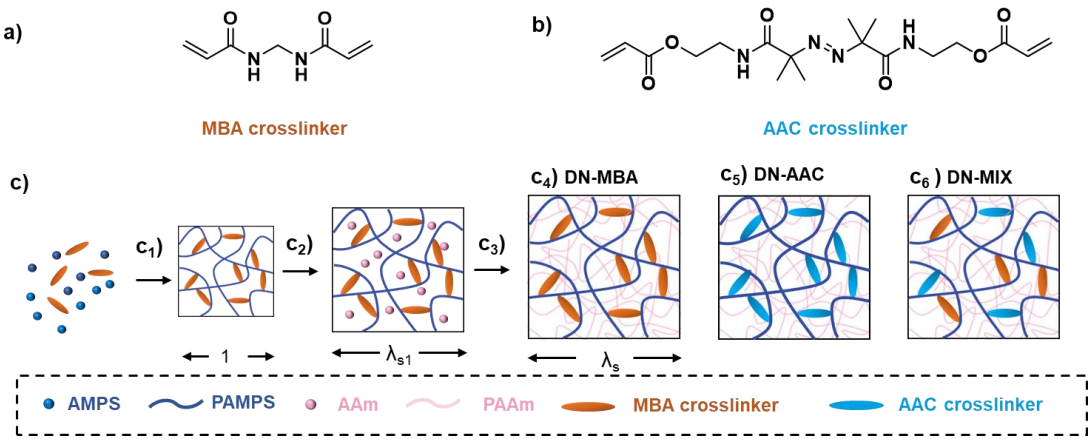

Figure 2.1. Preparation of DN gels with different crosslinkers. (a,b) Chemical structure of MBA (a) and AAC (b) crosslinkers. (c) By two step sequential polymerization (c_1-c_3) and varying the crosslinker in the first step of polymerization (c_1), DN gels with different crosslinkers (c_4-c_6) are synthesized: (c_1) synthesizing PAMPS SN gels, (c_2) immersing PAMPS SN gels in an acrylamide (AAm) solution, (c_3) synthesizing the second AAm network in PAMPS gels and then immersing them into pure water to obtain equilibrated DN gels (c_4-c_6).

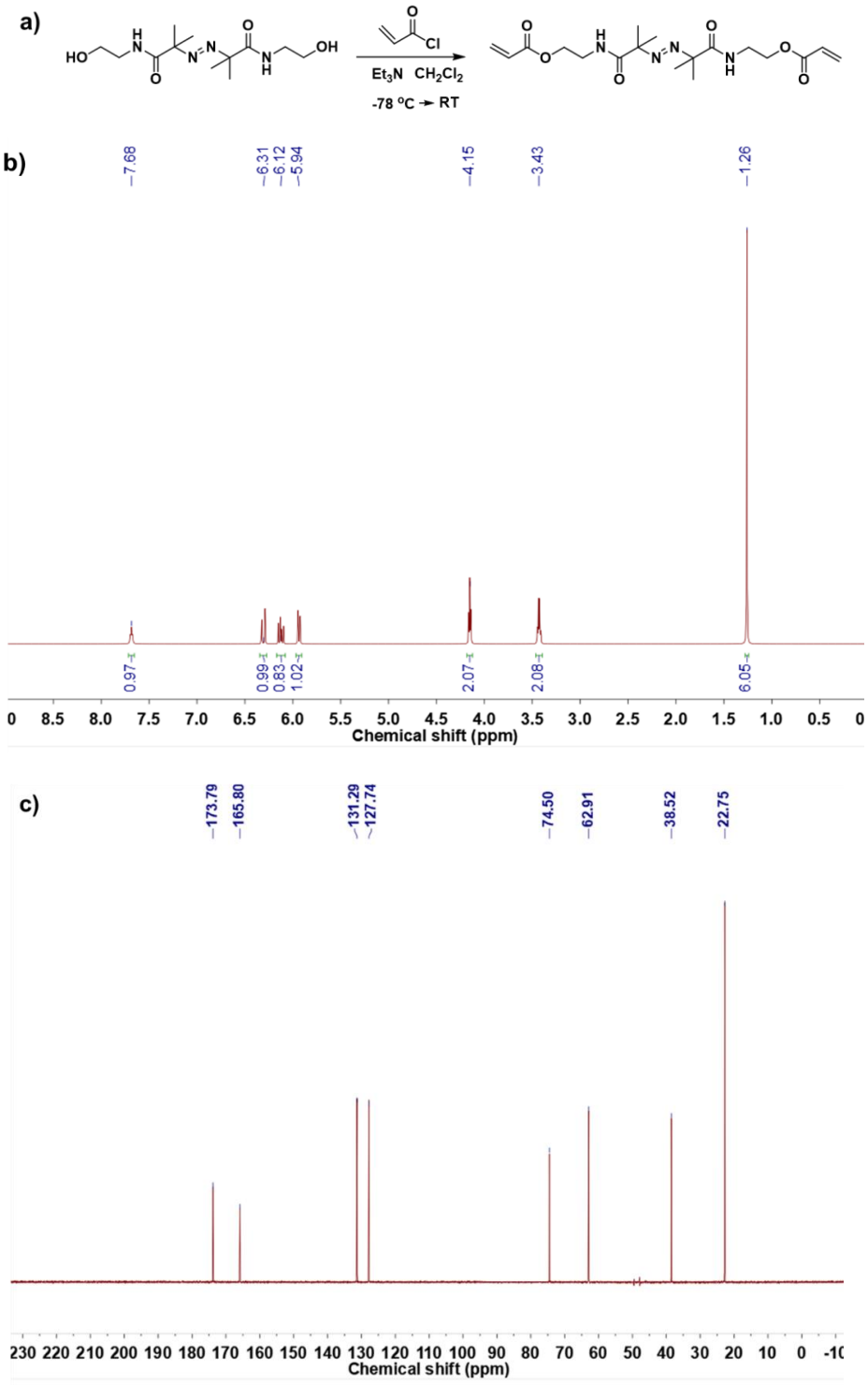

Figure 2.2. (a) Preparation of azoalkane crosslinker. (b) 1H NMR and (c) CNMR (500 MHz, DMSO) spectrum of the azoalkane crosslinker.

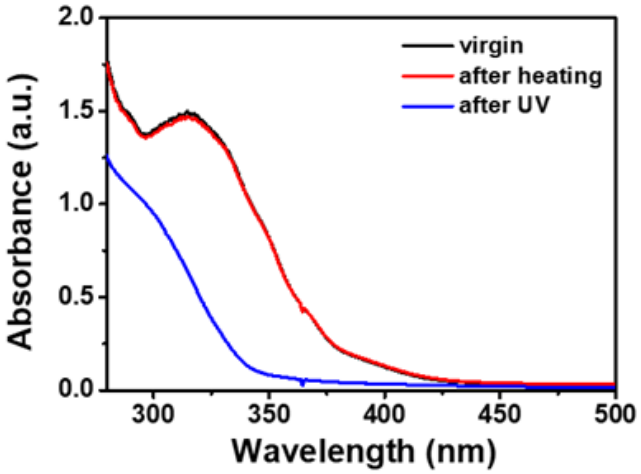

Figure 2.3. The UV-visible spectrum of azoalkane crosslinker (AAC) in DMF solution. Black: as-prepared AAC in DMF solution (0.01 g/ml). Red: after heating at 44℃ for 10 hours. Blue: after UV irradiation for 2 hours. AAC had the absorbance peak at 320 nm due to the azoalkane group. After exposed to UV light for 2 hours, the absorbance peak at 320 nm disappeared. In contrast, after heating at 44 ℃ for 10 hours, the absorbance at 320 nm kept almost constant, indicating the thermal decomposition of the AAC during the polymerizations can be negligible.

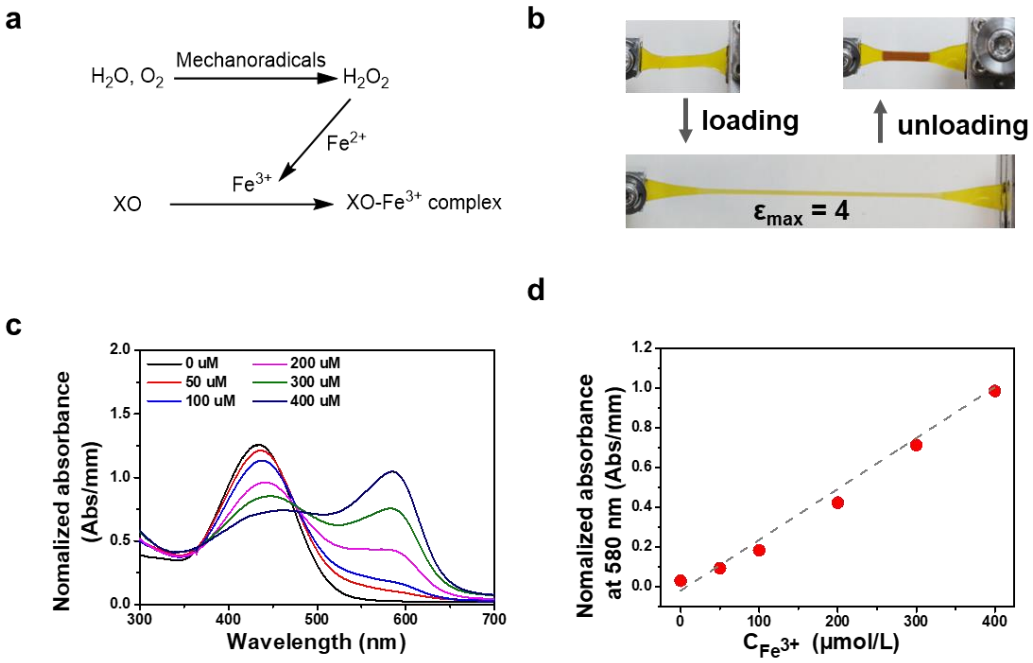

Figure 2.4. Quantification method of mechanoradical concentration of DN gels with different crosslinkers. (a) Fenton color reaction induced by mechanoradicals that makes yellow XO form purple XO-Fe^{3+} complex. (b) An example to show the color change before, during, after stretching of DN gels. (c) The UV-Vis spectrum of DN gels fed with a specified concentration of $NH_4Fe^{III}(SO_4)_2$ (0-500 μM), 500 μM $(NH_4)_2Fe^{II}(SO_4)_2$, 500 μM XO and 20 mM H_2SO_4. d) Calibration curve of normalized absorbance at 580 nm as a function of Fe^{3+} concentration fed to DN gels. The calibration curve is independent of the species of DN gels.

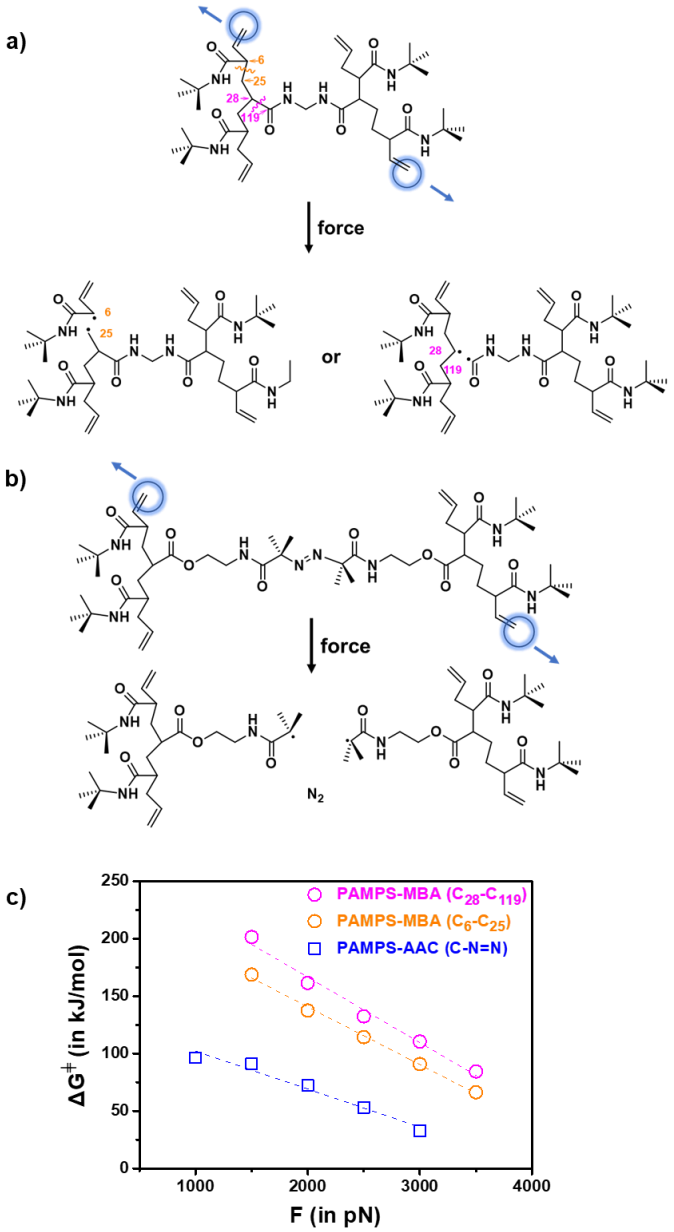

Figure 2.5. DFT simulation of the bond rupture under an external force. (a,b) Model molecule as the PAMPS-MBA (a) and PAMPS-AAC (b) network employed in the DFT calculations and corresponding generated mechanoradicals after bond rupture. Blue circle regions represent the fragments (i.e., CH_2 groups) of the molecule where artificial forces are added diagonally. (c) Relationship between the Gibbs energy barriers ($\Delta G^{\ddagger}$) of the covalent bond homolysis and the level of artificial tensile force (F).

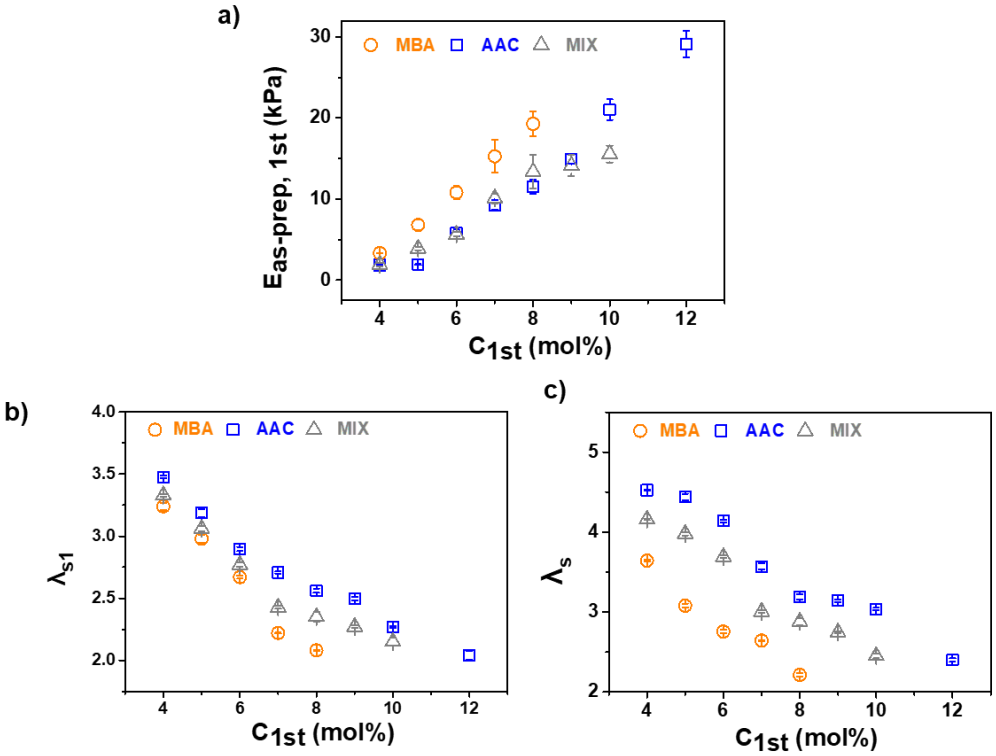

Figure 2.6. a) Young's modulus of as-prepared PAMPS SN gels $E_{as\text{-}prep,1st}$ with respect to the crosslinker concentration C_{1st}. b,c) The length swelling ratio of the three sets of PAMPS SN gels in the AAm monomer solution, λs_1, (b) and length swelling ratio of three sets of DN gels in water, λ_s, (c) with C_{1st}.

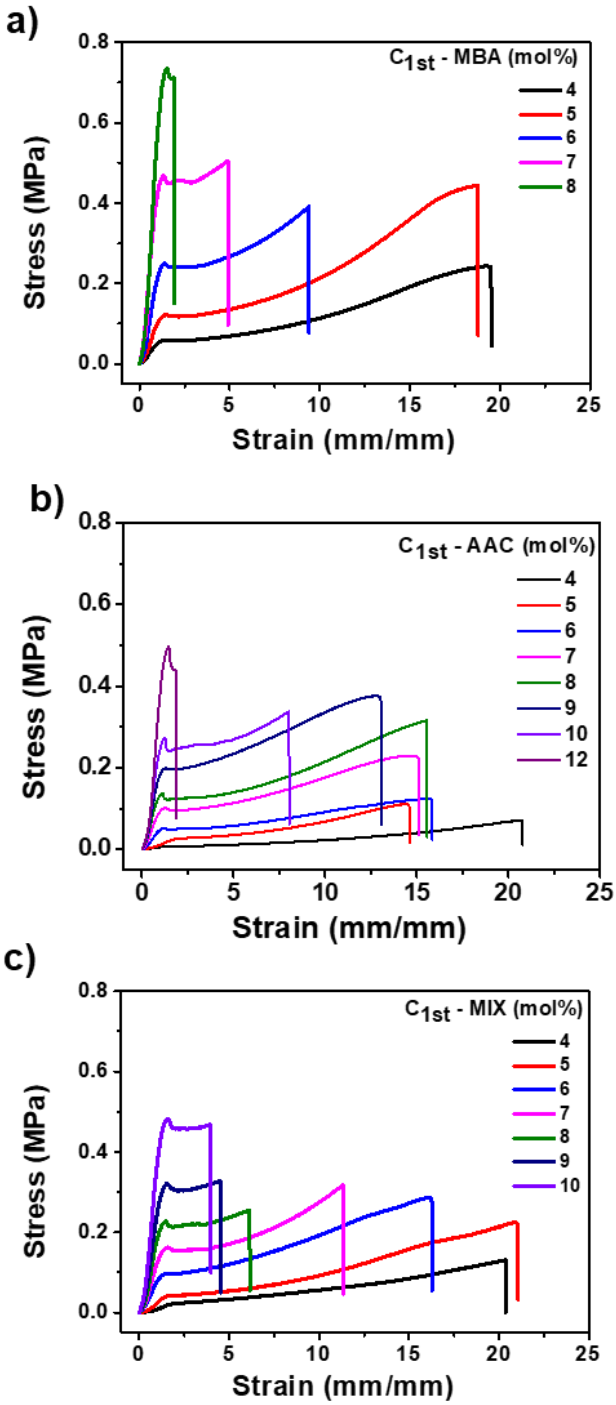

Figure 2.7. Tensile stress-strain curves of DN-MBA (a), DN-AAC (b), and DN-MIX (c).

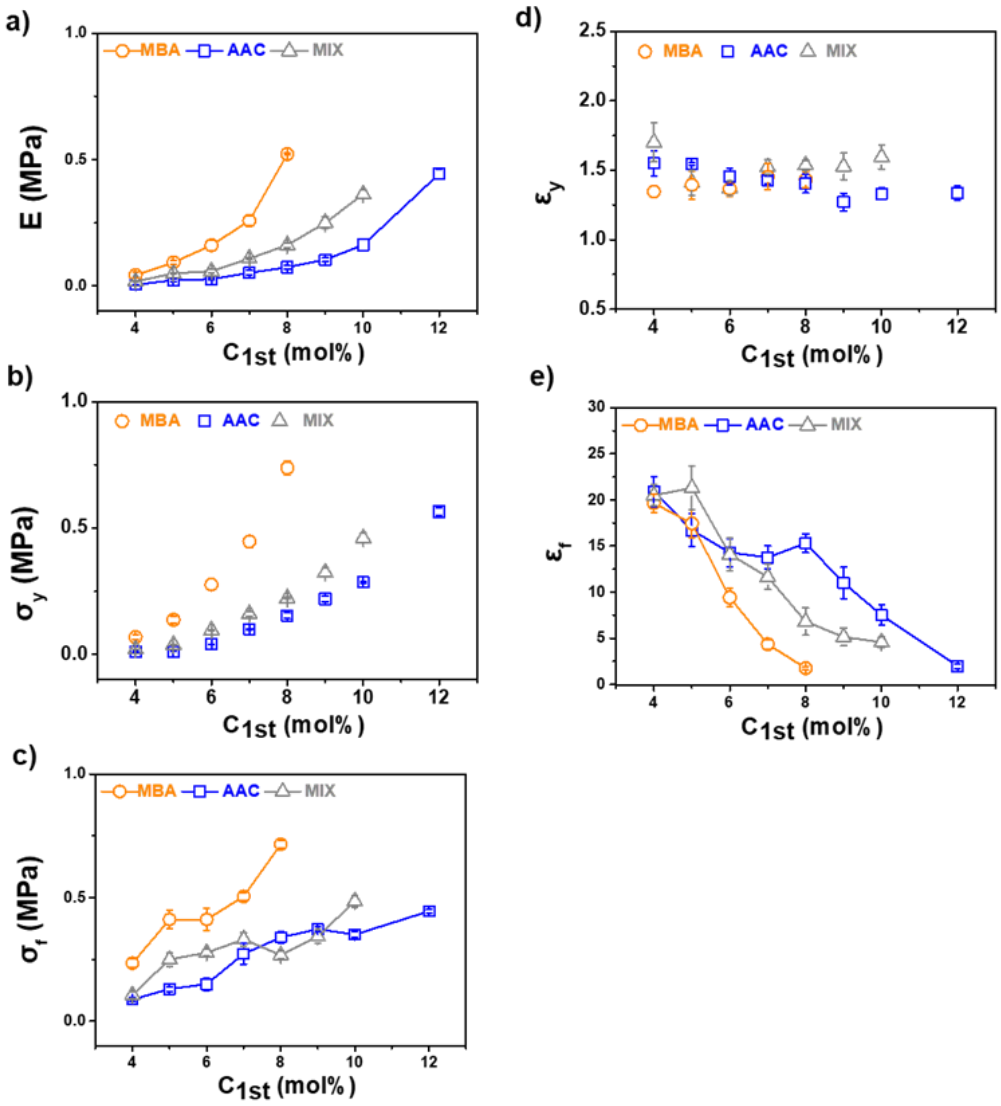

Figure 2.8. Statistics of the mechanical properties of three sets of DN gels. Young's modulus E (a), yield stress σ_y (b), fracture stress σ_f (c), yield strain ε_y (d) and fracture strain ε_f (e) of DN gels prepared with different in-feed concentration of crosslinkers C_{1st}.

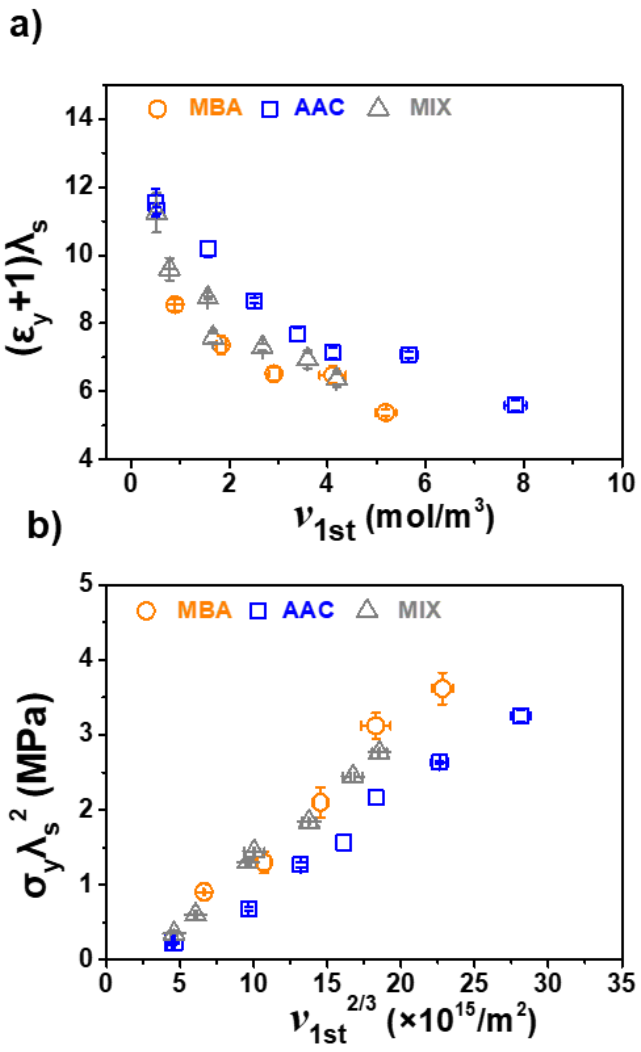

Figure 2.9. (a) Rescaled yield strain $(\varepsilon_y+1)\lambda_s$ with the effective crosslinking density of the PAMPS SN hydrogels $\nu_{1st.}$ (b) Rescaled yield stress $(\sigma_y\lambda_s^2)$ with the effective area crosslinking density of the PAMPS SN hydrogels $\nu_{1st}^{2/3}$.

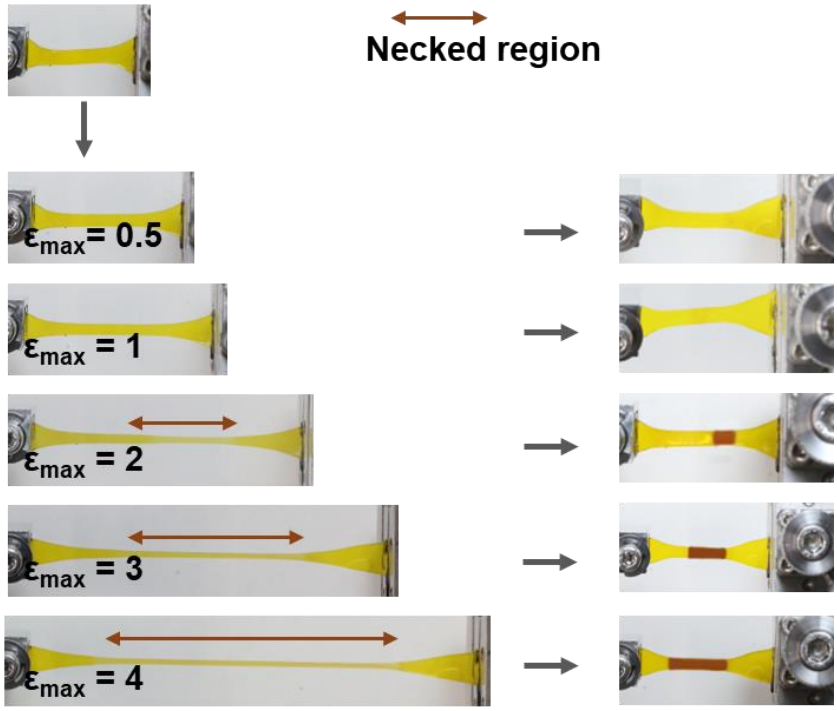

Figure 2.10. Photo images of DN-10AAC gels fed with $(NH_4)_2Fe^{II}(SO_4)_2$ and XO when stretched to different preset strain ε_{max}. Necking occurs at ε_{max}=1.2.

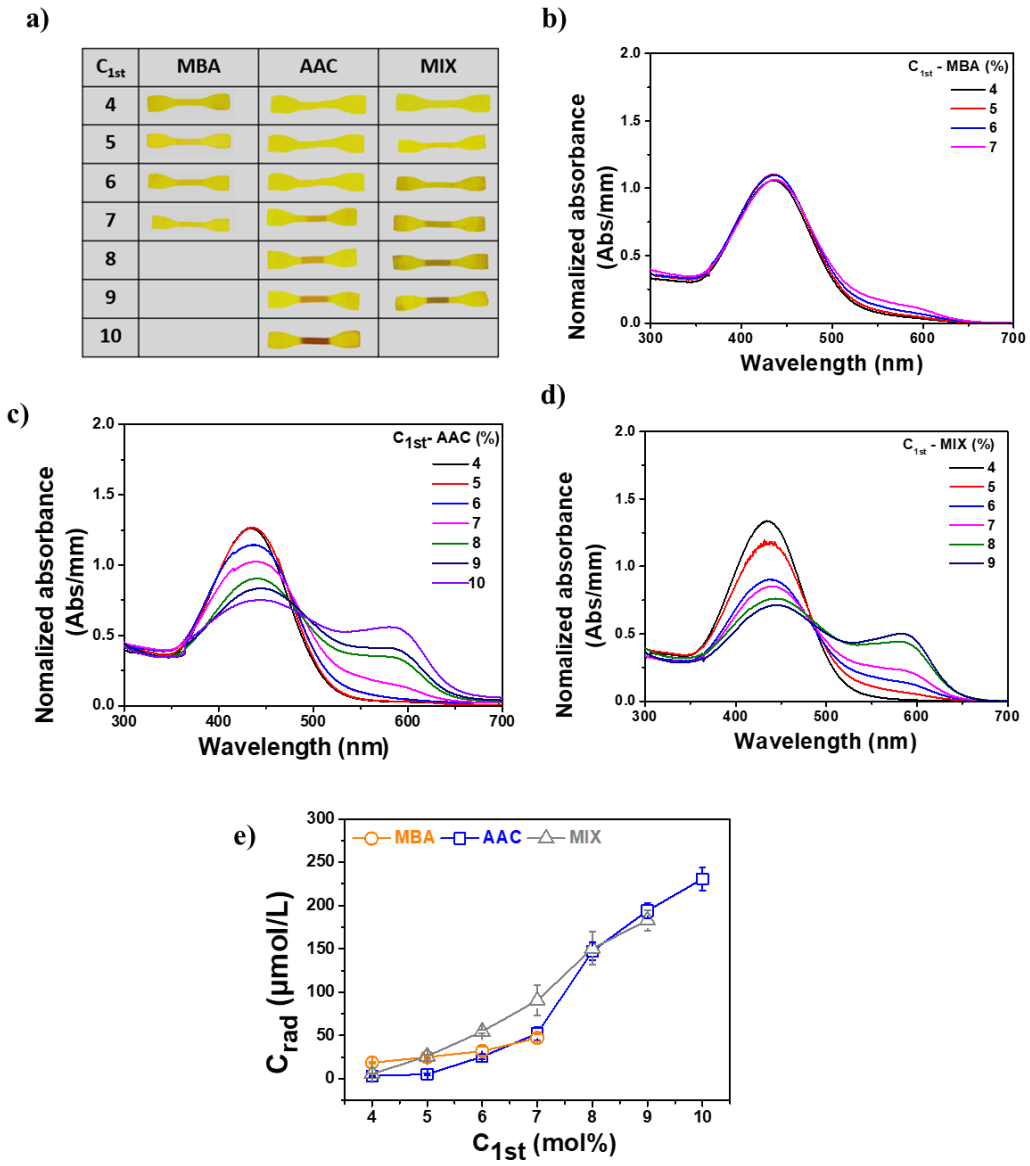

Figure 2.11. Characterization of mechanoradicals in DN gels after stretching by the Fenton color reaction. a) Photographic images of three sets of DN gels fed with Fe^{2+} and XO after stretching with respect to C_{1st}. b-d) UV-spectrum of DN-MBA (b), DN-AAC (c), DN-MIX (d) gels in the necked region after stretching to tensile strain at $\varepsilon_{max} = 4$. e) Mechanoradical concentration C_{rad} in the necked region of DN gels as a function of C_{1st}.

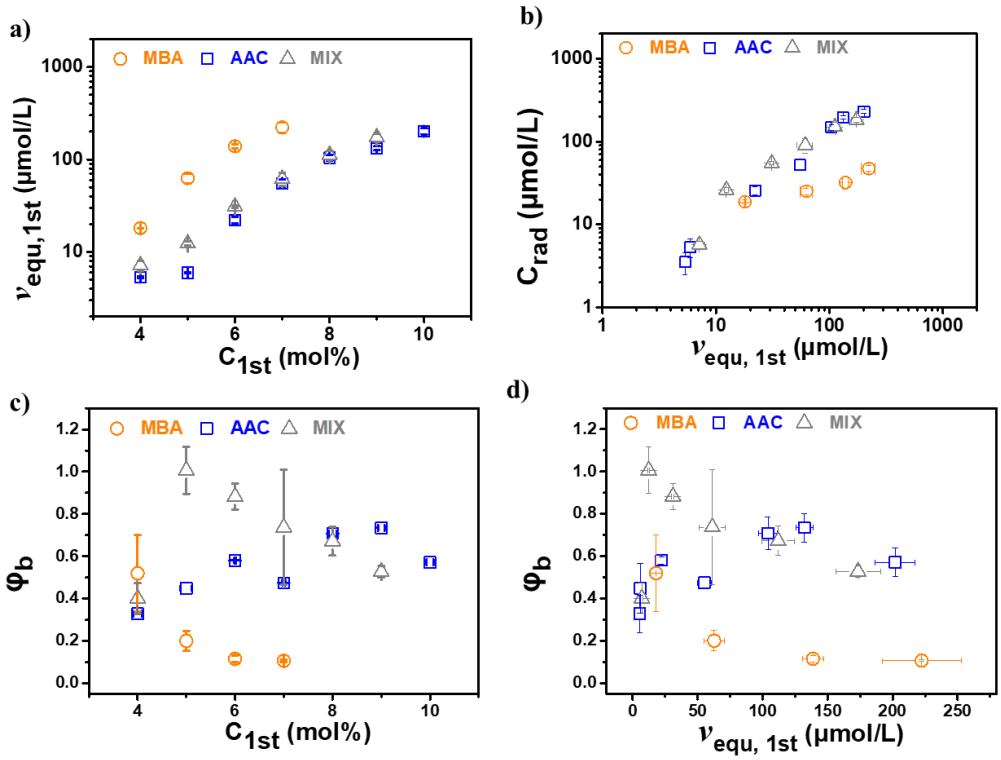

Figure 2.12. a) The PAMPS network density at swelling equilibrated state ($\nu_{equ,1st}$) as a function of C_{1st}. b) C_{rad} as a function of $\nu_{equ,1st}$. c,d) The ratio of broken strands to total strands of the PAMPS network φ_b, estimated from the relation of $\varphi_b = C_{rad}/(2\nu_{equ,1st})$, as a function of C_{1st} (c) and $\nu_{equ,1st}$ (d).

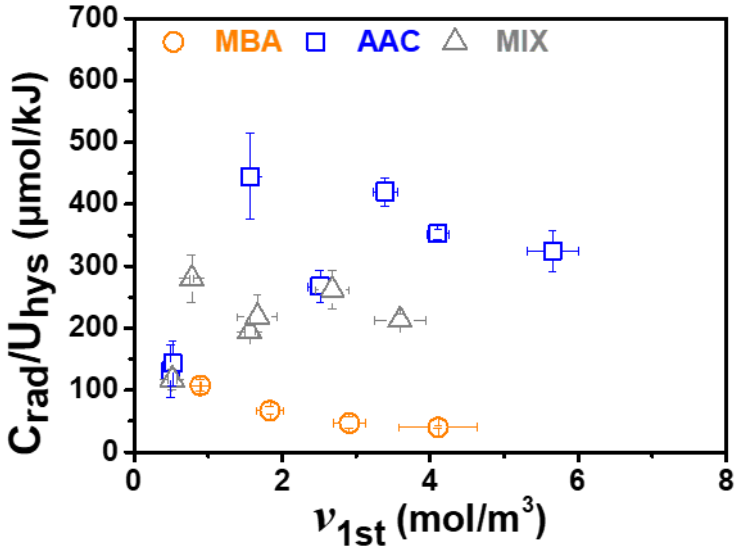

Figure 2.13. Energy efficiency for radical generation C_{rad}/U_{hys} as a function of the effective crosslinking density of the PAMPS SN hydrogels ν_{1st}.

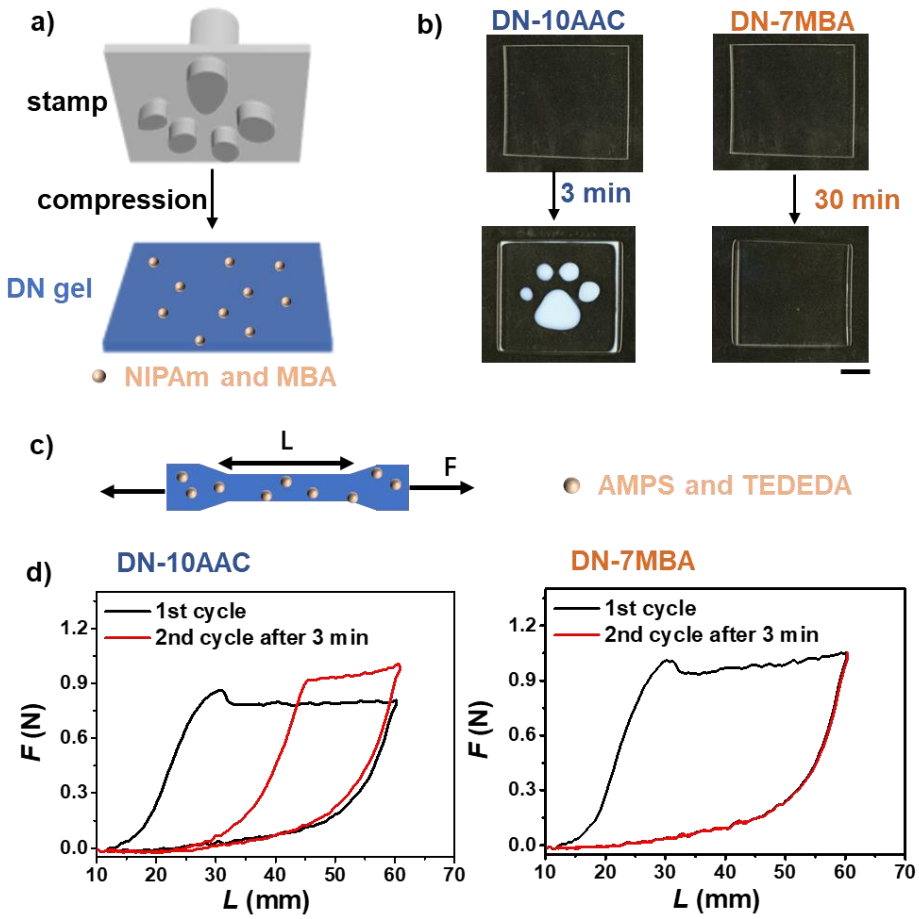

Figure 2.14. Fast force-responsive pattern (a,b) and strength enhancement (c,d) of DN gels with high mechanoradical concentration. (a) Illustration of DN gels fed with the monomer NIPAm and crosslinker MBA compressed by a stamp with a raised bear toe pattern. (b) Photographs of DN gels before and after compression. Scale bar: 1 cm. (c) Illustration of stretching DN gel with the supply of monomer AMPS and crosslinker TADETA. (d) Force-length curves showing the cyclic loading-unloading behavior of different DN gels. Black line: first cycle. Red line: second cycle.

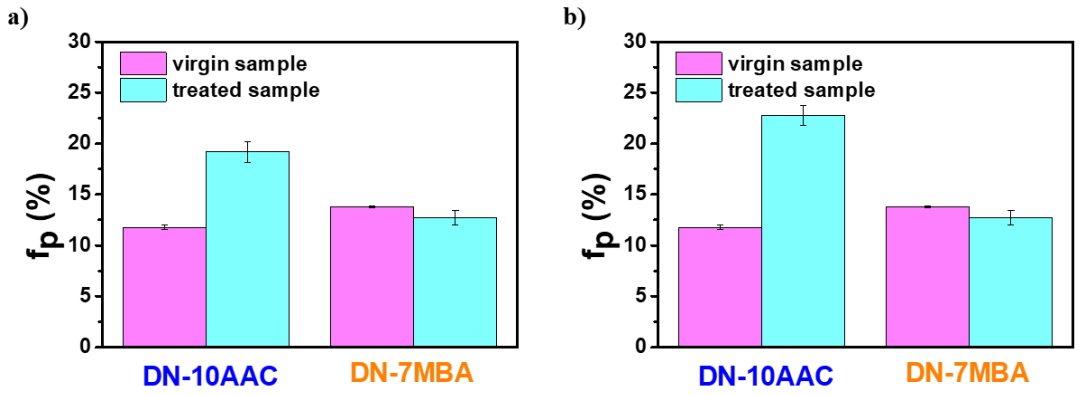

Figure 2.15. a) Polymer weight fraction f_p of DN-10AAC and DN-7MBA gels before and after compression when fed with NIPAm and MBA. b) f_p of DN-10AAC and DN-7MBA gels before and after stretching when fed with AMPS and TADETA. To test f_p of the gels after compression and after stretching, the gels in the compressed region and in the stretched region were cut and then immersed into a large amount of water for 2 days to remove unreacted monomers and crosslinkers.

2.5 References

1. Zavitsas, A. A. The relation between bond lengths and dissociation energies of carbon−carbon bonds. *J. Phys. Chem. A* **2003**, *107*, 897−898.
2. Li, J.; Nagamani, C.; Moore, J. S. Polymer mechanochemistry: from destructive to productive. *Acc. Chem. Res.* 2015, 48, 2181−2190.
3. Encina, M. V.; Lissi, E.; Sarasúa, M.; Gargallo, L.; Radic, D. Ultrasonic degradation of polyvinylpyrrolidone: effect of peroxide linkages. *J. Polym. Sci. Polym. Lett. Ed.* **1980**, *18*, 757–760.
4. Chen, Y. L.; Spiering, A. J. H.; Karthikeyan, S.; Peters, G. W. M.; Meijer, E. W. R.; Sijbesma, R. P. Mechanically induced chemiluminescence from polymers incorporating a 1,2-Dioxetane unit in the main chain. *Nat. Chem.* **2012**, *4*, 559–562.
5. Li, Y. C.; Nese, A.; Matyjaszewski, K.; Sheiko, S. S. Molecular tensile machines: anti-Arrhenius cleavage of disulfide bonds. *Macromolecules* **2013**, *46*, 7196–7201.
6. Lee, J.; Silberstein, M. N.; Abdeen, A. A.; Kim, S. Y.; Kilian, K. A. Mechanochemical functionalization of disulfide linked hydrogels. *Mater. Horiz.* **2016**, *3*, 447–451.
7. Berkowski, K. L.; Potisek, S. L.; Hickenboth, C. R.; Moore, J. S. Ultrasound-induced site-specific cleavage of azo-functionalized poly(ethylene glycol). *Macromolecules* **2005**, *38*, 8975–8978.
8. Lee, B.; Niu, Z. B.; Wang, J. P.; Slebodnick, C.; Craig, S. L. Relative mechanical strengths of weak bonds in sonochemical polymer mechanochemistry. *J. Am. Chem. Soc.* **2015**, *137*, 10826–10832.
9. Kim, G., Wu, Q., Chu, J.L., Smith, E.J., Oelze, M.L., Moore, J.S. and Li, K.C. Ultrasound controlled mechanophore activation in hydrogels for cancer therapy. *Proc. Natl. Acad. Sci.* **2022**, *119*, 21097911119.
10. Surampudi, S. K.; Patel, H. R.; Nagarjuna, G.; Venkataraman, D. Mechano-

isomerization of azobenzene. *Chem. Commun.* **2013**, *49*, 7519–7521.

11. Lin, Y. J.; Hansen, H. R.; Brittain, W. J.; Craig, S. L. Strain-dependent kinetics in the cis-to-trans isomerization of azobenzene in bulk elastomers. *J. Phys. Chem. B* **2019**, *123*, 8492–8498.
12. Davis, D. A.; Hamilton, A.; Yang, J.; Cremar, L. D.; Gough, D. V.; Potisek, S. L.; Ong, M. T.; Braun, P. V.; Martinez, T. J.; White, S. R.; Moore, J. S.; Sottos, N. R. Force-induced activation of covalent bonds in mechanoresponsive Polymeric materials. *Nature* **2009**, *459*, 69–72.
13. Kingsbury, C. M.; May, P. A.; Davis, D. A.; White, S. R.; Moore, J. S.; Sottos, N. R. Shear activation of mechanophore-crosslinked polymers. *J. Mater. Chem.* **2011**, *21*, 8381–8388.
14. Chen, Y. J.; Yeh, C. J.; Qi, Y.; Long, R.; Creton, C. From Force-responsive molecules to quantifying and mapping stresses in soft materials. *Sci. Adv.* **2020**, *6*, eaaz5093.
15. Chen, Y. J.; Sanoja, G.; Creton, C. Mechanochemistry unveils stress transfer during sacrificial bond fracture of tough multiple network elastomers. *Chem. Sci.* **2021**, *12*, 11098–1110.
16. Aubert, M.; Roth, M.; Pfaendner, R.; Wilén, C. E. Azoalkanes: a Novel class of additives for cross-linking and controlled degradation of Polyolefins. *Macromol. Mater. Eng.* **2007**, 292, 707–714.
17. Maeda, S.; Ohno, K.; Morokuma, K. Systematic exploration of the mechanism of chemical reactions: the global reaction route mapping (GRRM) strategy using the ADDF and AFIR Methods. *Phys. Chem. Chem. Phys.* **2013**, *15*, 3683–3701.
18. Maeda, S.; Harabuchi, Y. Exploring paths of chemical transformations in molecular and periodic systems: an approach utilizing force. *WIREs Comput. Mol. Sci.* **2021**,

11, e1538.

19. Rubinstein, M.; Colby, R. Polymer Physics, *OUP Oxford*, **2003**, pp 262−266.
20. Ahmed, S.; Nakajima, T.; Kurokawa, T.; Haque, M. A.; Gong, J. P. Brittle-ductile transition of double network hydrogels: mechanical balance of two networks as the key Factor. *Polymer* **2014**, *55*, 914–923.
21. Nakajima, T.; Kurokawa, T.; Furukawa, H.; Gong, J. P. Effect of the constituent networks of double network gels on their mechanical properties and energy dissipation process. *Soft Matter* **2020**, *16*, 8618–8627.
22. Matsuda, T.; Nakajima, T.; Fukuda, Y.; Hong, W.; Sakai, T.; Kurokawa, T.; Chung, U. I.; Gong, J. P. Yielding criteria of double network hydrogels. *Macromolecules* **2016,** *49*, 1865–1872.
23. Nakajima, T.; Kurokawa, T.; Ahmed, S.; Wu, W. L.; Gong, J. P. Characterization of internal fracture process of double network hydrogels under uniaxial elongation. *Soft Matter* **2013**, *9*, 1955–1966.
24. Lake, G. J.; Thomas, A. G. The strength of highly elastic materials. *Proc. R. Soc. Lond. A* **1967**, *300*, 108–119.

Chapter 3: Hydrogel morphogenesis induced by force-controlled growth

3.1 Introduction

The morphological characteristics of biological systems develop through their growth, which is often triggered by mechanical forces[1-4]. Taking early embryogenesis[1,2] as an example (**Figure 3.1a**), the accumulation of fluid inside the embryo leads to an increase in hydraulic pressure. Hydraulic pressure causes the embryo to expand to a large size and change in shape. Meanwhile, this mechanical force weakens the cell-cell junction, resulting in further cell proliferation and rearrangement in the presence of a nutrient supply from the mother. Thus, the embryo attains growth in size, shape development, and mechanical strength simultaneously.

Hydrogels, a class of materials that show structure and property similarity to soft biological tissues, however, sometimes are difficult to be reshaped once formed. It is because most hydrogels are chemically crosslinked and thus show elastic deformation (i.e. temporary and self-recoverable). Recent years have seen the development of shape shifting hydrogels through dynamic non-covalent or dynamic covalent crosslinking bonds[5-8]. However, to achieve plastic deformation (i.e., permanent and non-self-recoverable) in the solid state, these hydrogels require pre-treatment such as heating and UV to soft the gel and post-treatment such as cooling to fix the gel shape. Besides, these reshaping processes don't involve the synthesis of the new mass into the system and resultant growth in size and stiffness.

How can we apply biological growth-based morphogenesis mechanism to hydrogel materials?[9,10] In this chapter, by using an azo-crosslinked DN gel with high concentration of mechanoradicals, we develop a strategy for hydrogel morphogenesis through force-controlled growth (**Figure 3.1b**). Applying a mechanical force to the DN gel causes its deformation, along with the bond rupture and mechanoradical generation in the brittle network. By supplying monomers to the gel, the mechanoradicals triggered the formation of a new network inside the deformed gel. When the new network density is sufficiently high, it can counterbalance the retraction of the original network and maintain the force-induced deformation permanently. In other words, this new network confers plasticity to the elastic gel. With this plasticity, we can adopt an existing shaping process for solids, such as the blowing or drawing processes for plastics and metals, to transform rapidly two-dimensional gel sheets into various three-dimensional shapes at room temperature.

The key point of this strategy is to ensure the high-density network formed in the deformed gels to fix the shape deformation. For this purpose, we adopt DN gels with their first network crosslinked by 10 mol% AAC (DN-10AAC) and supply to these DN gels with 2-acrylamido-2-methyl-1-propanesulfonic acid (AMPS) monomers in the presence of MBA crosslinkers. The high mechanoradical concentration in DN-10AAC gels and high concentration of supplied monomers and crosslinkers would likely ensure a high polymerization rate and high network density. More importantly, we extend the time duration of force application to maintain the deformed state during the mechanoradical polymerization. This is the main difference compared with the work in

chapter 2 and in the reference 10.

3.2 Experiments

3.2.1 Materials

DN gels with their first network crosslinked by 10 mol% AAC (defined as DN-10AAC) were fabricated by following the method described in **section 2.2.3.** The mechanoradical concentration generated in DN-10AAC is ~220 uM.

For demonstrating the importance of high concentration of mechanoradicals, DN gels with their first network crosslinked by 7 mol% MBA (defined as DN-7MBA) were also fabricated. The mechanoradical concentration generated in DN-7MBA is ~40 uM.

3.2.2 Shape retention ratio of the stretched DN gels

The DN-10AAC gels that were 1.45 mm in thickness were immersed in a monomer solution containing 2.0 M AMPS and 0.15 M MBA for 1 d to reach the equilibrium state. Then, they were cut into dumbbell-shaped strips (12 mm in gauge length and 2 mm in width). Subsequently, the dumbbell-shaped DN gels in the solution were placed in a glove box with argon for 2 h to remove the oxygen. The gels containing monomers and crosslinkers were then stretched to a preset value of strain ε_{max} at a velocity of 100 mm/min. The samples were stretched in water instead of the corresponding monomer solution to reduce the amount of monomer used. After different dwell times, t, the gels were unloaded to observe the residual strain, $\varepsilon_{r.}$ For comparison, the same stretching experiments were performed on DN-10AAC gels without monomers, DN-10AAC gels containing other monomers and MBA, and DN-7MBA gels containing AMPS and

MBA.

3.2.3 Measurement of polymer weight fraction of the gels

The polymer weight fraction of the gels (fp) was measured by following the method described in **section 2.2.9**.

3.2.4 Measurement of width and modulus after different dwell time

DN-10AAC gels of 1.45 mm-thickness were immersed in a monomer solution containing 2.0 M AMPS and 0.15 M MBA for one day to reach the equilibrium state. Then the gels were cut into dumbbell-shaped strips (12 mm gauge length and 2 mm width). After that, dumbbell-shaped DN gels in the solution were put into an argon glove box for 2 hours to remove oxygen. The gels containing monomers and crosslinkers then were stretched in water to a preset strain $\varepsilon_{max} = 4$ by a handheld clamping device. After different dwell time t (t = 0, 1,3,7,10,15 min), the samples were immediately removed from water and taken out from the glove box. The samples were still fixed on the clamping device to measure the width by a polarized optical microscope (Lv100 pol, Nikon Co.). To measure the modulus of the gels after different dwell time, the samples were unloaded and new gauge length and width at the unloading state were measured. Then unloaded samples were conducted tensile test immediately to obtain the modulus of the samples. For a comparison, the same experiments were performed on DN-10AAC gels without monomers and crosslinkers.

3.2.5 Forming by drawing and blowing

The DN-10AAC gels of 2.9 mm-thickness were cut into rectangular stripes (50 mm

in length and 5 mm in width) for drawing or square sheets (50 mm in length and 50 mm in width) for blowing. The cut gels were immersed in a monomer solution of 2.0 M AMPS and 0.15 M MBA for 1 day to reach equilibrium. Subsequently, the gels in the solution were placed in a glove box with for 2 h to remove the oxygen. For the drawing process, the rectangular-shaped gel strips were quickly stretched until their complete necking by hand and then immediately fixed around a cubic object or glass rod, or twisted by hand, to obtain the designed shape. The gels were then immersed in the monomer solution for 15 min to fix the shape. Subsequently, the two ends of each gel were trimmed to obtain the final reshaped gels. For the free blowing process, the square-shaped gel sheets were clamped tightly between two plastic plates, with a hole with a designed shape in the center of the top plate. Then, the monomer solution (approximately 5-7 mL) was injected into the confined region between the gel and the bottom plate using a needle, to blow the gel through the hole into the target shape. The gels were then immersed in the monomer solution for 15 min to fix the shape. Subsequently, the periphery of each gel was trimmed to obtain the gels with the designed hollow shapes.

3.3 Results and Discussion

3.3.1 Plasticity of DN gels by mechanoradical polymerization

To achieve the hydrogel morphogenesis directly regulated by the external, the key challenge is to confer the plasticity to the elastic DN gels. The plasticity of the DN-10AAC gels is investigated by tensile tests with loading-dwelling-unloading cycles

using dumbbell-shaped gel samples. As shown in **Figure 3.2a**, the samples were stretched to a preset value of strain (ε_{max}). After maintaining the load for different dwell times (t, min), the external force was removed and the residual strain (ε_r) was recorded. The plasticity of each specimen was characterized by the shape retention ratio relative to the stretched state, $R_f = (\varepsilon_r/\varepsilon_{max}) \times 100\%$.

First, we compared the mechanical behaviors of the DN-10AAC gels with and without monomers (M) and crosslinkers (C) fed prior to the stretching (**Figure 3.2b-d)**. After stretching the sample to a point near its complete necking ($\varepsilon_{max} = 4$) followed by immediate unloading (dwell time t = 0 min), the DN-10AAC gel without monomers and crosslinkers recovered its original length almost completely ($\varepsilon_r = 0.1$, $R_f = 2.5\%$) because of the elasticity of the PAAm network (**Figure 3.2b, d** and **Figure 3.4a**). The extension of the dwell time to 15 min only slightly increased the residual strain ($\varepsilon_r = 0.5$, $R_f = 12.5\%$) because of water redistribution following the internal damage of the brittle network. The destruction of the PAMPS network caused by force resulted in a remarkable decrease in the modulus (**Figure 3.3a**).

In comparison, a DN-10AAC gel containing monomers and crosslinkers (2.0 M AMPS and 0.15 M MBA) subjected to the same loading and immediate unloading process did not recover its initial shape and showed a large permanent residual strain ($\varepsilon_r = 1.8$, $R_f = 48\%$). This indicates that the stress-induced mechanoradicals have triggered the polymerization of AMPS and MBA to form a new network during the loading and unloading process. By extending the dwell time from 0 to 15 min, the shape retention ratio of the gel increased from 48% to 90%, showing nearly full plasticity at

15 min (**Figure 3.2c, d**). The effect of the dwell time on R_f is due to the progress of crosslinking in the sample being dwelled, which is also suggested by the increase in modulus during dwelling (**Figure 3.3a, Figure 3.4b**) and by the fact that the sample with only monomers and no crosslinkers showed a small R_f (**Figure 3.5**). The modulus of the sample subjected to a dwell time of 15 min with a newly formed network was 170 times that of the stretched sample without new network formation. Thus, the newly formed network is robust enough to counterbalance the elasticity of the PAAm network, which remains in a highly stretched state even after removing the external force (**Figure 3.6**).

During the loading-unloading process, the size of the samples changed simultaneously (**Figure 3.3b**). The rapid loading process resulted in a decrease in the sample width owing to the incompressibility of the sample. However, during the dwelling process, the sample with monomers and crosslinkers exhibited a large increase in width with dwell time, indicating that the osmotic pressure of the newly formed network induces a volume increase in the gel. The stretched pre-existing network counterbalances the swelling of the newly formed network along the elongation direction, so that the gel only swells along the direction perpendicular to that. The sample without monomers and crosslinkers also showed moderate lateral swelling caused by the fracture of the brittle network[11]. In addition, the polymer weight fraction (f_p) of the self-grown gel was approximately three times higher than that of the original sample (**Figure 3.3c**). Thus, the plasticity of the DN-10AAC hydrogels achieved through the new structural growth is accompanied by an increase in strength, volume,

and polymer weight fraction. This is different from the plasticity found in conventional materials, in which the mass and volume remain constant before and after the deformation.

A high plasticity (high value of R_f) can only be obtained when a large number of mechanoradicals are generated in the gel. This is clearly shown by the dependence of R_f on the tensile strain ε_{max} (**Figure 3.7**). R_f increases with ε_{max} above the value of ε_{max} = 0.5, where the mechanical hysteresis of the DN gel starts to appear and saturates to a value as high as ~ 90% for values of ε_{max} above the yield point of the gel (ε_y = 1.2). The importance of high mechanoradical concentration for high plasticity is also shown by the results of the DN-7MBA gels, where the brittle network is crosslinked with MBA. The DN-7MBA gel hardly showed any plasticity, even at values of strain above the yield point, owing to its low mechanoradical concentration (**Figure 3.8**).

The plasticity induced in DN gels by mechanoradical polymerization is common for diverse monomers (**Figure 3.5**). This was shown by a set of experiments in which the DN-10AAC gels were fed with various monomers (2.0 M) and an MBA crosslinker (0.15 M). After the loading-dwelling-unloading treatment (ε_{max} = 4, t = 15 min), all the DN-10AAC gels showed plasticity. However, the shape retention ratio R_f depends on the monomer species. When the DN-10AAC gels contained a mixture of AMPS and acrylamide monomers (molar ratio 1:1), a high plasticity with $R_f \approx 90\%$ was obtained, similar to that obtained with only AMPS monomers. Partial plasticity with R_f ranging from 20% to 63% was observed in monomer solutions of acrylamide, acrylic acid, 2-acryloxyethyltrimethylammonium chloride, and *N*-isopropylacrylamide.

3.3.2 Morphogenesis induced by force-controlled growth of DN-10AAC gels

Since DN-10AAC gels containing monomers and crosslinkers exhibit nearly full plasticity due to the formation of a new network with a high modulus after the stretching, we first applied free blowing and blow molding[12,13] to reshape 2D gel sheets in the form of complex hollow configurations, mimicking the morphogenesis of an embryo, as illustrated in **Figure 3.1**. A gel sheet containing monomers and crosslinkers was clamped tightly between two plates, with the top plate containing a pre-designed hole in the center. Through a needle fixed between the gel sheet and the bottom plate, a monomer solution (2.0 M AMPS, 0.15 M MBA) was injected into the confined space. The gel was thus blown through the hole to form the designed hollow shape (**Figure 3.9**). The high stretchability of the DN gels makes it feasible to inflate the gel sheet by hydraulic pressure. Blowing induces biaxial stretching of the gel sheet, which triggers the formation of new networks that fix the blown shape. As shown in **Figure 3.9b and 3.9ci**, if the gel sheets are freely blown through a circular hole, hollow, flask-shaped hydrogels can be produced. By changing the shape of the hole in the top plate, various complex configurations can be achieved, such as a tridimensional love heart shape (**Figure 3.9cii**), a bull-head-like shape (**Figure 3.9ciii**), and an octopus-like shape (**Figure 3.9civ**). To form non-spherical shapes that cannot be obtained by free blowing, a mold was placed on top of the hole to restrict the expansion of the gel. The gel sheet was blown into the mold cavity to cover the interior wall, so that it adopted the shape of the mold. By applying the corresponding molds, the gel sheets formed a hollow Mongolian yurt shape (**Figure 3.9cv**), and a hollow truncated cone shape with an

external thread transferred from the mold (**Figure 3.9cvi**). It should be noted that, owing to the mechanical constraints of the top plate, the tensile strain is position-dependent, leading to a thickness gradient on the final gel shape.

We can also apply other existing processes for metal reshaping to reshape the gel in the solid state directly by applying an external force at room temperature. Metal and plastic forming technologies[14], such as bending, drawing, and rolling, could also be applicable to gels. For example, a rectangular gel strip was stretched (drawing) to its complete necking (**Figure 3.10a**) and then immediately deformed into a pre-designed shape (bending). After maintaining the deformed state in the monomer solution for 15 min to allow the formation of a new network, the designed shape was permanently fixed. Using this protocol, by wrapping a stretched sample around a cuboid object or a cylindrical glass rod, we obtained a gel in the shape of a square ring (**Figure 3.10b**) or helical strip (Figure **3.10c**), respectively. By twisting a stretched sample, we obtained a gel with a twisted shape (**Figure 3.10d**). In addition to the above configurations, other morphing structures can be easily attained with the assistance of the corresponding equipment. Compared with time-consuming 3D printing, these plastic forming processes are suitable for high-efficient manufacturing the low-cost objects using hydrogels.

3.4 Conclusion

We show hydrogel morphogenesis through force-triggered growth in the DN gels. The use of weak sacrificial crosslinker to generate mechanoradicals in high

concentrations and the extension of dwell time are key factors in obtaining plasticity. By adopting different industrial processing technologies, one-dimensional gel strips and two- dimensional gel sheets can be reshaped into various configurations in the solid state by directly applying an external force at room temperature, with no other treatment of the samples. This work provides an effective way to obtain elastic hydrogels with various 3D shapes, particularly those with hollow structures. The core of this morphogenesis strategy is forced-induced destructive bond scissors and further constructive bond formations. Thus, this strategy should be applied to other multi-network materials containing sacrificial bonds[15] and other synthetic materials that can undergo mechano-responsive reconstruction reactions[16-19]. In addition, new functions could be conferred to the gels during the morphogenesis process by using appropriate monomers for the growth, further extending the application of the materials.

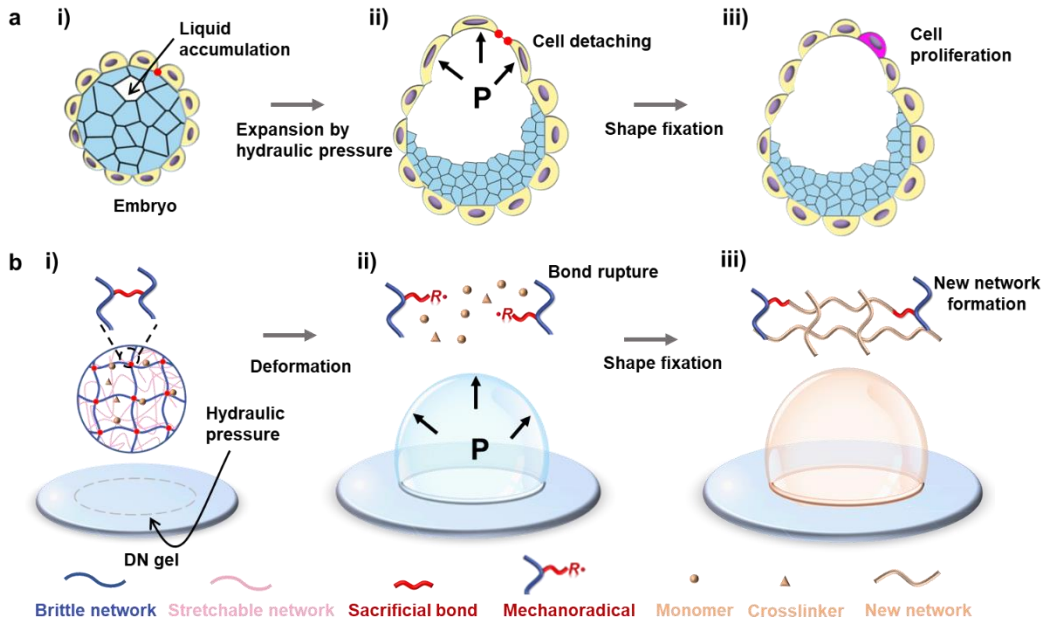

Figure 3.1. Conceptual scheme of the biomimetic hydrogel morphogenesis induced by force-controlled growth. a) An example of early morphogenesis of an embryo. (a-i) hydraulic pressure is generated inside an embryo; (a-ii) the hydraulic pressure P weakens the cell-cell junction and induces the size increase and deformation of the embryo; (a-iii) the embryo grows maintaining the shape through cell proliferation and rearrangement. b) Our strategy for achieving hydrogel morphogenesis by force-controlled growth in a double network hydrogel (DN gel). (b-i) A DN gel with a brittle network crosslinked with sacrificial crosslinkers; (b-ii) the brittle network breaks by bond scission of the sacrificial crosslinkers upon deformation and generates a high concentration of mechanoradicals; (b-iii) the gel gains morphological plasticity through the mechanoradical polymerization of monomers supplied from the external environment. As an example, a gel expansion induced by hydraulic pressure is illustrated. The detailed description of the experimental setup is shown in **Figure 3.9**.

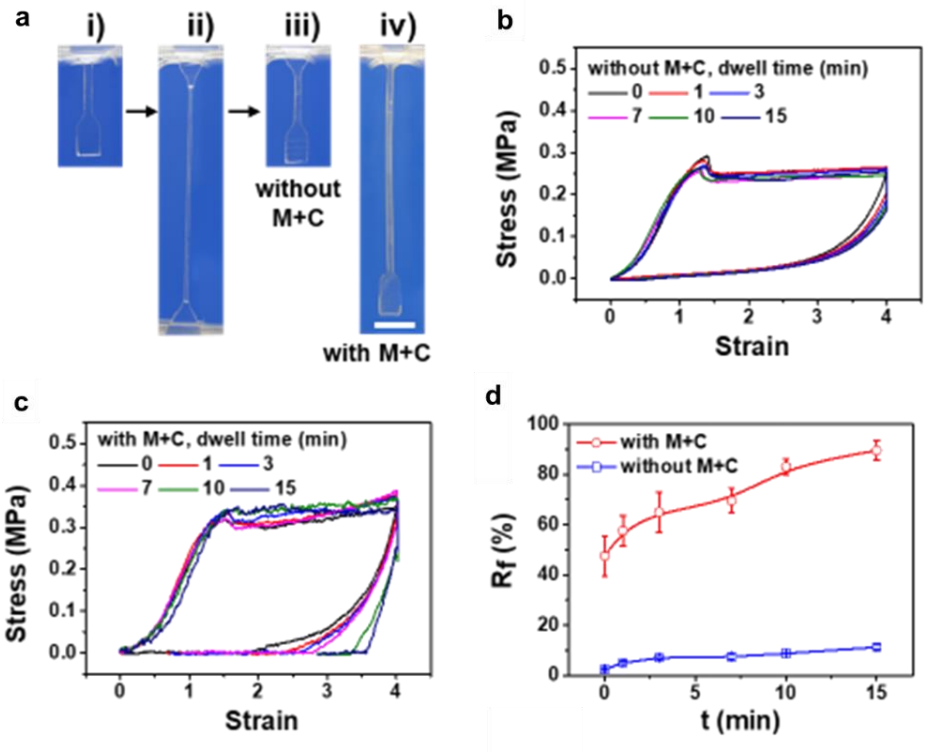

Figure 3.2. Plasticity of DN-10AAC gels fed with monomers (M) and crosslinkers (C). a) (i-iii) Photo images of the samples without M+C before loading (i), during dwelling (ii), and after unloading (iii). (iv) photo image of the samples with M+C after the whole treatment. Scale bar: 1 cm. b, c) Cyclic tensile stress-strain curves of the samples without M+C (b) and with M+C (c) with different dwell times t. d) Shape retention ratio (R_f) as a function of the dwell time t.

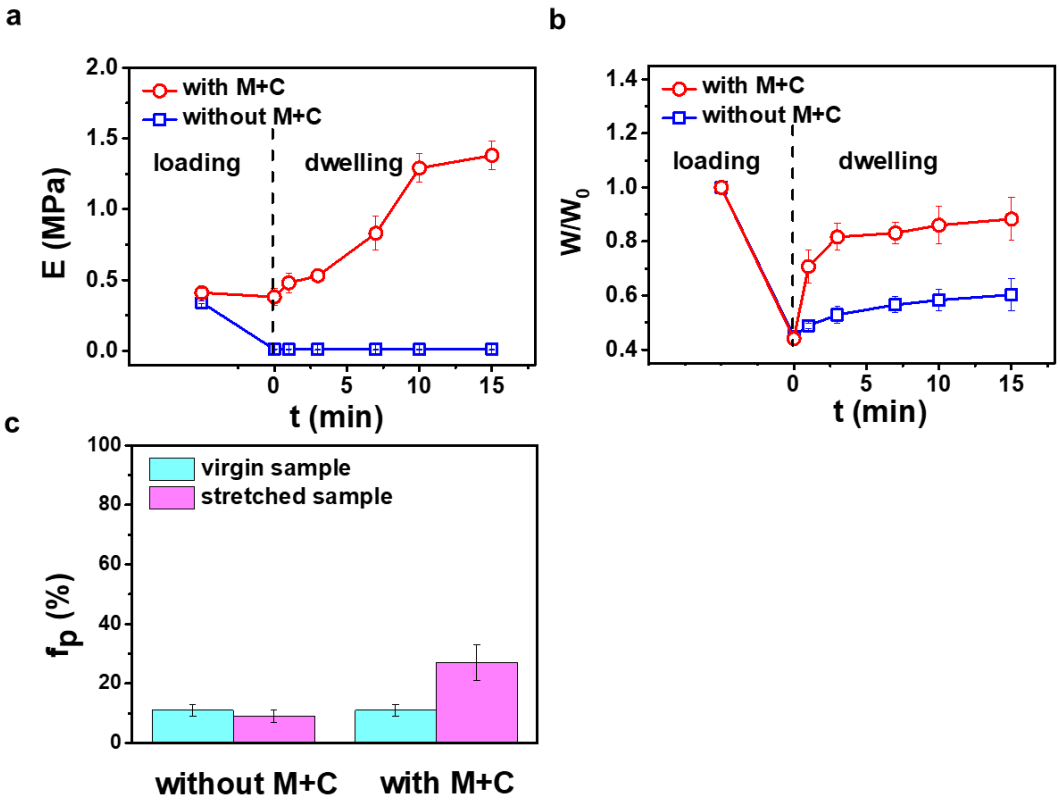

Figure 3.3. a, b) Changes in the modulus E (a) and relative width (W/W_0) (b) during the treatment, where W and W_0 are the current sample width and the original width before loading, respectively. c) polymer weight fraction (f_p) of the samples before and after the cyclic loading with a dwell time of 15 min.

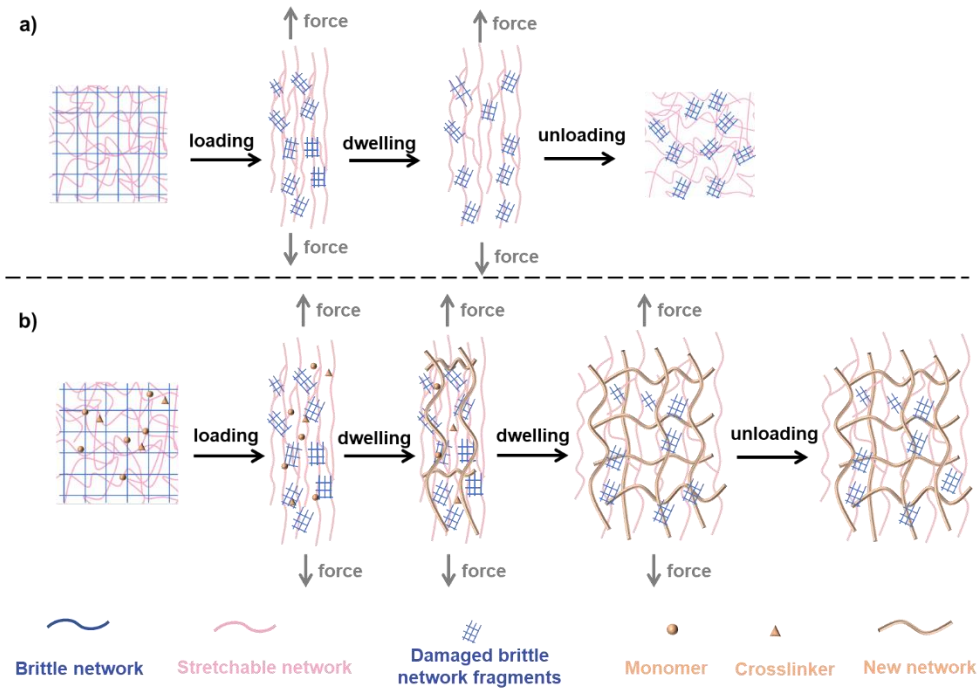

Figure 3.4. Illustration of the structure change of DN-10AAC gels fed without (a) and with (b) monomers and crosslinkers during the loading-dwelling-unloading treatment.

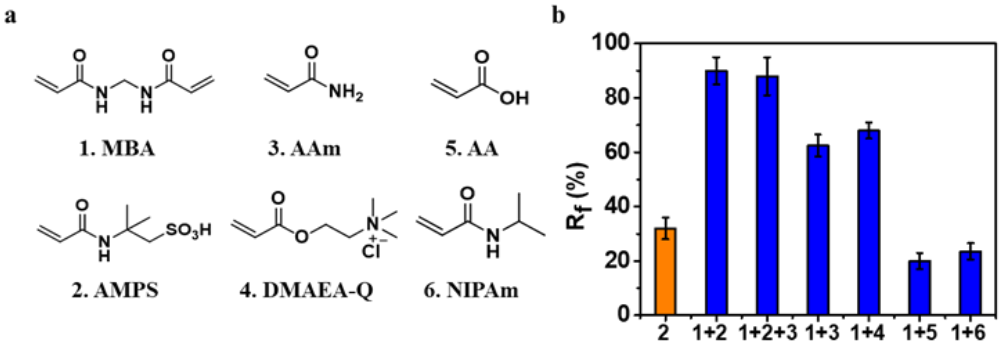

Figure 3.5. Effect of monomers and crosslinkers fed to the DN-10AAC gels on the shape retention ratio Rf. a) Chemical structure of different monomers and crosslinkers. b) Shape retention ratio R_f as a function of monomer varieties. The total monomer concentration was 2.0 M and the MBA crosslinker was 0.15 M. Dwell time t was kept 15 min. The shape retention ratio of the DN-10AAC gels only containing monomers yet no crosslinkers (2.0 M AMPS) is also demonstrated in orange column, the value of which is about ~30%.

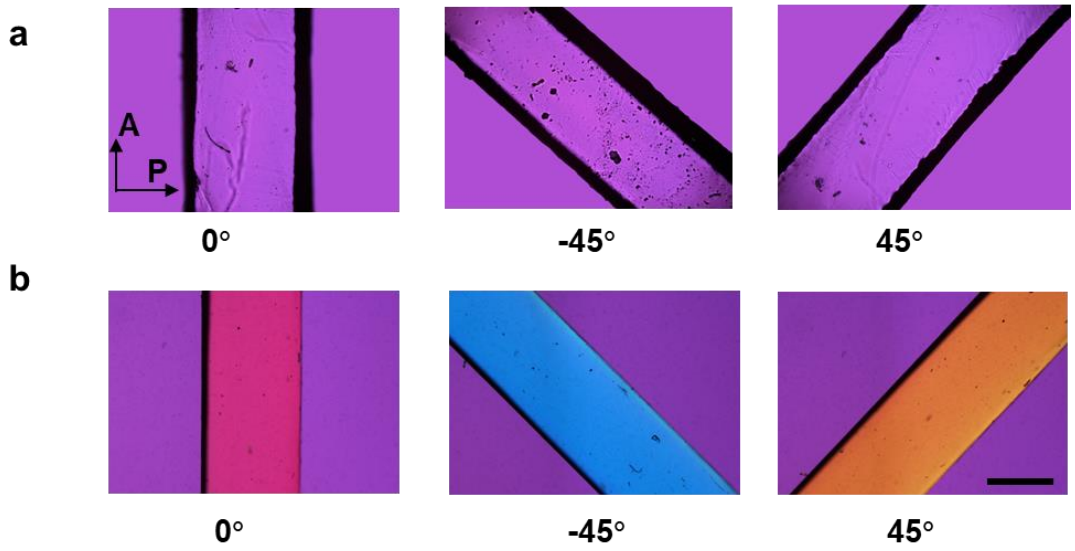

Figure 3.6. Polarized optical microscope (POM) images with a 530 nm tint plate of DN-10AAC gels after prolonged stretching (stretching strain ε_{max} = 4, dwell time t= 15 min) (a) without and (b) with AMPS monomers (2.0 M) and MBA crosslinkers (0.15 M). The POM was performed at unloaded state. A: analyzer; P: polarizer. The 530 nm tint plate can sensitively indicate the molecular orientation of the gel through the color change. Scale bar: 1 mm.

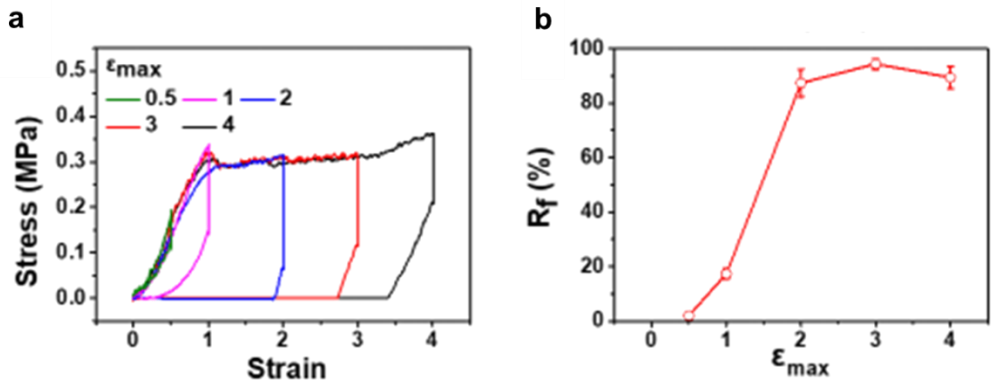

Figure 3.7. a) Cyclic tensile stress-strain curves of DN-10AAC gels containing monomers and crosslinkers stretched to different preset values of strain (ε_{max}). b) Resultant shape retention ratio R_f as a function of ε_{max}. The dwell time was 15 min.

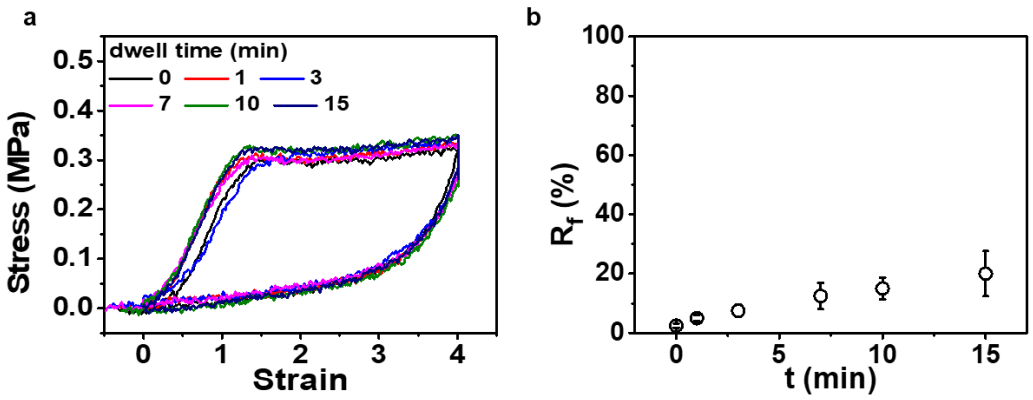

Figure 3.8. Tensile stress-strain curves of DN-7MBA gels fed with AMPS monomers (2.0 M) and MBA crosslinkers (0.15 M) (a) and the resultant shape retention ratio R_f (b) for different dwell time.

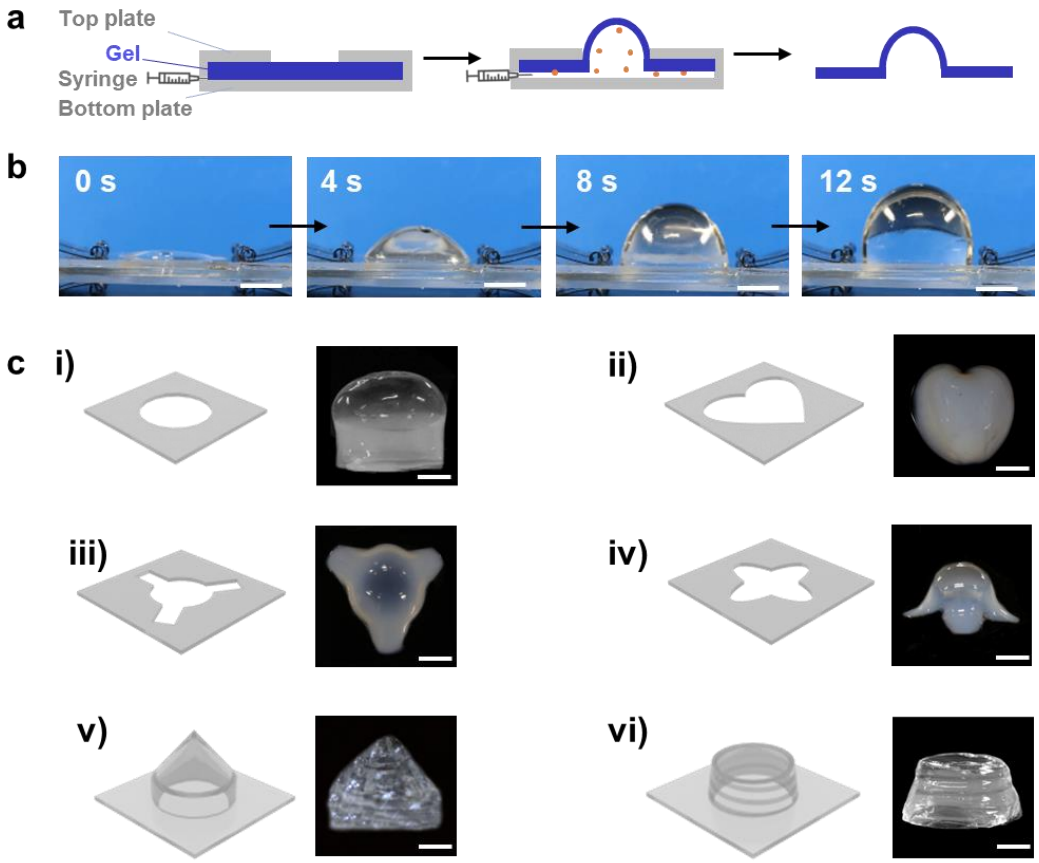

Figure 3.9. Morphogenesis of DN-10AAC gels by blowing triggered growth. a) Illustration of the forming process by blowing. A piece of DN gel sheet is sandwiched between two plastic plates. The top plate has a designed hole in the center (left). A monomer solution is injected into the confined space between the gel and the bottom plate to blow the gel by hydraulic pressure, through the hole and into the pre-designed shape (middle). The growth-induced plasticity fixes the shape (right). b) Images showing the rapid deformation process of the gel as it is freely blown through the top plate with a circular hole. c) Illustrations of top plates with various pre-designed holes (left) and photo images of the corresponding gels (right) reshaped by free blowing (i-iv) and mold blowing (v-vi). Scale bar: 1 cm.

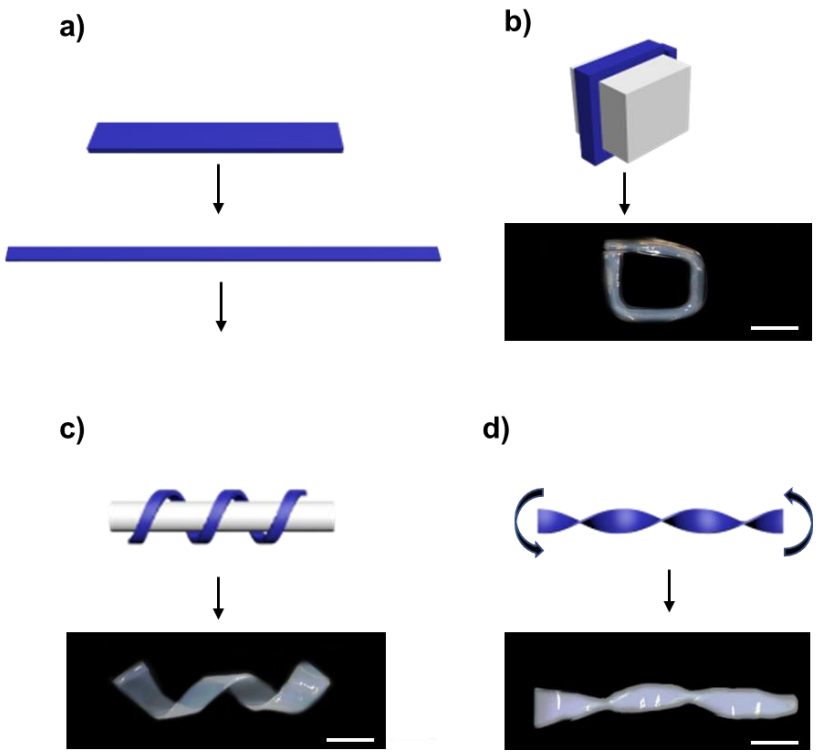

Figure 3.10. Morphogenesis of DN-10AAC gels by drawing and bending forming. A strip of DN gel is stretched to its complete necking (a) and then immediately formed into different shapes to obtain the reshaped hydrogels (b-d). See details in Methods. Scale bar: 1 cm.

3.5 References

1. Valet, M., Siggia, E. D., Brivanlou, A. H. Mechanical regulation of early vertebrate embryogenesis. *Nat. Rev. Mol. Cell Biol.* **2022,** *23*, 169-184.
2. Chan, C. J., Maria, C., Teresa, R., Gregor, M., Ryar, M., Takashi, H. Hydraulic control of mammalian embryo size and cell fate. *Nature* **2019**, *571*, 112-116.
3. Cosgrove, D. J. Growth of the plant cell wall. *Nat. Rev. Mol. Cell Biol.* **2015**, *6*, 850. 850-861.
4. Bassel, G.W., Stamm, P., Mosca, G., de Reuille, P.B., Gibbs, D.J., Winter, R., Janka, A., Holdsworth, M.J. Smith, R.S. Mechanical constraints imposed by 3D cellular geometry and arrangement modulate growth patterns in the Arabidopsis embryo. *Proc. Natl Acad. Sci.* **2014**, *111*, 8685-8690.
5. Zhu, C. N., Bai, T., Wang, H., Ling, J., Huang, F., Hong, W., Zheng, Q., Wu, Z. L. Dual-encryption in a shape-memory hydrogel with tunable fluorescence and reconfigurable architecture. *Adv. Mater.* **2021**, *33*, 2102023.
6. Shang, J., Le, X., Zhang, J., Chen, T., Theato, P. Trends in polymeric shape memory hydrogels and hydrogel actuators. *Poly. Chem.* **2019**, *10*, 1036-1055.
7. Chakma, P., Konkolewicz, D. Dynamic covalent bonds in polymeric materials. *Angew. Chem.* **2019**, *131*, 9784-9797.
8. Ni, C., Chen, D., Zhang, Y., Xie, T., Zhao, Q. Autonomous shapeshifting hydrogels via temporal programming of photoswitchable dynamic network. *Chem. Mater.* **2021**, *33*, 2046-2053.
9. Xiong, X., Wang, S., Xue, L., Wang, H., Cui, J. Growing strategy for postmodifying

cross-linked polymers' bulky size, shape, and mechanical properties. *ACS Appl. Mater. & Interfaces*, **2022**, *14*, 8473-8481.

10. Matusda, T., Kawakami, R., Namba, R., Nakajima, T., Gong, J. P. Mechano-responsive self-growing hydrogels inspired by muscle training. *Science* **2019**, *363*, 504-508.
11. Nakajima, T.; Kurokawa, T.; Ahmed, S.; Wu, W. l.; Gong, J. P. Characterization of internal fracture process of double network hydrogels under uniaxial elongation. *Soft Matter* **2013**, *9*, 1955−1966.
12. Wirthl, D., Pichler, R., Drack, M., Kettlguber, G., Moser, R., Gerstmayr, R., Hartmann, F., Bradt, E., Kaltseis, R., Siket, C. M., Schausberger, S. E., Hild, S., Bauer, S., Kaltenbrunner, M., Instant tough bonding of hydrogels for soft machines and electronics. *Sci. Adv.* **2017**, *3*, e1700053.
13. Jones, T. J., Jambon-Puillet, E., Marthelot, J., Brun, P. T. Bubble casting soft robotics. *Nature*, **2021**, *599*, 229-233.
14. Chatterjee, R., Mukhopadhyay, J. A review of super plastic forming. *Mater. Today Proc.* **2018**, *5*, 4452-4459.
15. Ducrot, E., Chen, Y., Bulters, M., Sijbesma, R. P., Creton, C. Toughening elastomers with sacrificial bonds and watching them break. *Science* **2014**, *344*, 186-189.
16. Li, J., Nagamani, C., & Moore, J. S. Polymer mechanochemistry: from destructive to productive. *Acc. Chem. Res.* **2015**, *48*, 2181-2190.
17. Kida, J., Aoki, D., & Otsuka, H. Self-strengthening of cross-linked elastomers via the use of dynamic covalent macrocyclic mechanophores. *ACS Macro Lett.* **2021**,

10, 558-563.

18. Ramirez, A. L. B., Kean, Z. S., Orlicki, J. A., Champhekar, M., Elsakr, S. M., Krause, W. E., Craig, S. L. Mechanochemical strengthening of a synthetic polymer in response to typically destructive shear forces. *Nat. Chem.* **2013**, *5*, 757-761.
19. Wang, Z., Wang, J., Ayarza, J., Steeves, T., Hu, Z., Manna, S., & Esser-Kahn, A. P. Bio-inspired mechanically adaptive materials through vibration-induced crosslinking. *Nat. Mater.* **2021**, *20*, 869-874.

Chapter 4: Enhanced crack resistance of double network hydrogels via mechanoradical polymerization in the crack tip

4.1 Introduction

The crack resistance of the soft gels and elastomers, typically characterized as fracture toughness[1-3], is essential for the practical applications of these materials. The cracks in the materials may be introduced intentionally or unintentionally during fabrication or formed during use. These cracks will cause the early fracture of the materials along the crack tip due to the stress concentration and resultant complex activities near the crack tip, involving chain elongation and orientation, chain pull-out, and bond breaking[4-6]. Whereas intrinsically hydrogels have low fracture toughness due to the low polymer density and high water content[7], tough hydrogels have been achieved through several strategies[7-16] regarding the activities around the crack tip, such as reducing the force on the polymer strands via dense entanglements[9], dissipating the input energy via sacrificial structures[10-13], or enhancing the crack tip via hierarchical structure[14,15] and strain-induced crystallization[16].

Driven by the need to further enhance the crack resistance of hydrogels, we focus on the bond breaking near the crack tip and its generated mechanoradicals to enhance the crack tip via mechanoradical polymerization. We choose double network (DN) hydrogel as an example to demonstrate this strategy due to their large damage zone ahead of the crack tip[17,18] and resultant high concentration of mechanoradicals in the damage zone[18]. As shown in **Figure 4.1**, when the material with a crack is subject to an

applied force, stress concentrates at the crack tip, causing the chain elongation and bond breaking of first network. With the presence of the monomers and crosslinkers, mechanoradicals generated by the bond breaking trigger the polymerization of monomers to form a new network. The newly formed network is able to reinforce the crack tip to delay the crack initiation, in other words, to increase the fracture toughness of the materials. This strategy should be suitable for other polymer materials[19,20] and should work well together with the other strategy to increase the fracture toughness.

In this chapter, we only adopted azoalkane-crosslinked DN gels for experiments, in which the mechanoradical concentration generated in the DN gel can reach ~200 μM. It should be noted that the abbreviation behind the DN in this chapter doesn't mean the crosslinker species in the first network, instead, it means the monomer species or just water fed to the azoalkane-crosslinked DN gels. To realize the fast formation of a new strong network near the crack tip, the azo-crosslinked DN gels were pre-immersed into the (2-(acryloyloxy)ethyl) trimethylammonium chloride (DAC) in presence with MBA to reach the equilibrium. Such DN gels containing DAC and MBA inside the gel are denoted as DN-DAC while DN gels without monomers and crosslinkers are denoted as DN-H_2O.

Concentrated DAC and MBA in DN-DAC slightly shrank the gel (**Table 4.1**) but themselves didn't change the mechanical behavior of the DN gel. DN-DAC gel showed the almost same behavior as the DN-H_2O gel when stretched in air (**Figure 4.2**). Thus, we mainly compare the different mechanical behavior between DN -DAC gel and DN-H_2O gel in the argon glove box when performed the uniaxial tensile test, single edge

notched test, trouser tearing test, and pure shear test at the different loading rates (from 10 mm/min to 300 mm/min due to the machine limitation). We demonstrate the enhanced crack resistance effect via mechanoradical polymerization was rate dependent. The real-time birefringence observation was applied to observe the damage zone during the test (**Figure 4.3**).

4.2 Experiments

4.2.1 Preparation of the hydrogels

The DN gels with their first network crosslinked by 9.5 mol% AAC were fabricated by following the method described in **section 2.2.3**. The slight decrease of crosslinker concentration compared with the work in chapters 2 and 3 (10 mol%) is for obtaining better stretchability and resultant better demonstration effect. The mechanoradical concentration generated in this gel is about ~200 μM.

The synthesized as-prepared DN gels were then swelled in a large amount of water to remove the residual. Such DN gels are defined as the DN-H_2O. The thickness of the DN-H_2O gel was 1.45 mm. DN-H_2O hydrogels were cut into pieces with different sizes and shapes by laser cutter for the following mechanical measurements (**Figure 4.4**).

The size of those cut DN-H_2O gels which need to be immersed in different monomer solutions is enlarged by a factor of (1/*f*), where *f* is the shrinkage ratio in length of DN-H_2O gel in different monomer solutions (**Table 4.1**). For example, the shrinkage ratio of DN-H_2O gels when immersed into the DAC monomer (2.0 M) solution with the presence of MBA (0.15 M) was 0.95. To prepare a notched dumbbell-shaped gel with

gauge length L of 20 mm, gauge width W of 10 mm, crack length c of 1 mm, the DN-H_2O gel was cut by laser cutter with L= 20 * (1/0.95) = 21.05 mm, W = 10 * (1/0.95) = 10.52 mm, c = 1 * (1/0.95) =1.05 mm. Then this cut gel was immersed into the DAC monomer solution to reach the equilibrium state. Such DN gels are defined as the DN-DAC gels. To study the influence of monomer varieties fed to the DN-H_2O gels, cut DN-H_2O gels were immersed into different monomer solutions (NaAMPS, NIPAm, or AAm; 2.0 M) with the presence of the MBA (0.15 M, crosslinker) to reach the equilibrium state following the same procedure.

4.2.2 Mechanical tests

The cut DN-H_2O gels, DN-DAC gels, and other DN gels fed with various monomers were placed in an argon glove box for 2 hours to remove oxygen. The cut gels with corresponding geometry were then performed tensile tests, single edge notched tests, pure shear tests, and tearing tests at a loading rate from 10 mm/min to 300 mm/min using a commercial tensile tester (MCT-2150, A&D Co.).

For comparison, these cut gels were directly stretched in air using a commercial tensile (Instron 5965, Instron Co.).

4.2.3 Methods of dyeing

In single edge notched tests, notched DN-DAC hydrogels were stretched into the different maximum stretch ratios and then unloaded. Unstretched DN-DAC gels (control) and stretched DN-DAC gels were immersed in a large amount of water for 2 days to remove the unreacted monomers. Then DN-DAC gels were immersed into the

methyl blue water solution (0.05 mg/mL) for one day to dye the region where polyDAC network formed. The dyed samples were immersed into water to remove the unbound methyl blue for observation.

In pure shear test and tearing test, fractured DN-DAC gels were performed the same dyeing procedure.

4.3 Results and Discussion

4.3.1 Uniaxial tensile test

Uniaxial tensile tests were performed prior to the fracture test with the real-time birefringence observation system. The birefringence images help reveal the chain orientation and stress distribution during deformation[21]. **Figure 4.5** shows the stress-stretch ratio (σ-λ) curves and **Figure 4.6** shows the statistics data of DN-H_2O and DN-DAC in the argon glove box at the different loading rate. DN-H_2O gel showed stress yielding which corresponded to the onset of necking in the sample. Necking phenomenon was induced by the extensive fracture of the first PAMPS network whereas the second PAAm network preserved the integrity of the gel. As stretch ratio increased above necking, relatively large amounts of strain localized in the softened necked region. This caused PAAm network in the necked region highly stretched and orientated along the tensile direction, which resulted in strong birefringence (**Figure 4.7a**). Since no time-consuming activities were involved during the deformation, the tensile behavior of DN-H_2O was almost rate-independent at the loading rate (v) from 10 mm/min to 300 mm/min (**Figure 4.5 and 4.6**)[22]. The necking of DN-H_2O gel started

at stretch ratio $\lambda \sim 2.4$ and completed at $\lambda \sim 5.2$. The fracture stress (σ_f) was 0.45 MPa and fracture stretch ratio (λ_f) was about 10.

In contrast, DN-DAC gels showed interesting two-section rate-dependent behavior. σ-λ curves before the yield point overlapped with the DN-H_2O and were rate-independent, while σ-λ curves after the yield point deviated from the DN-H_2O with decrease of the loading rate (**Figures 4.5 and 4.6**). Such two-section rate-dependent behavior was caused by the fact that high concentration mechanoradicals were only generated in the necked region after reaching the yield stretch ratio $\lambda_y \sim 2.4$. Within the stretch ratio λ from 1 to 2.4, there are few mechanoradicals generated in the gel and thus no new network formation to influence the mechanical behavior. Above the $\lambda_y \sim 2.4$, mechanoradicals generated in the necked region can trigger the polymerization and crosslinking of DAC and MBA to form a new network, in which crosslinking process was a relatively slow process[23]. At v = 300 mm/min, the loading time of the gel from yield point to fracture was about 0.5 min, which was too short to form an effective network in the DN-DAC gel. Thus, DN-DAC showed almost similar tensile behavior with the DN-H_2O gel at the whole range of the stretch ratio at this loading rate. With the decrease of the loading rate and resultant increase of the loading time, new network gradually forms to enhance the necked region, which made necking extension completed at the smaller stretch ratio of $\lambda \sim 2.7$ (**Figure 4.7b**). As a result, DN-DAC gel showed the increase in fracture stress and the decrease in fracture stretch ratio with decrease of the loading rate. The σ-λ curves of DN-DAC at v = 30 mm/min and v = 10 mm/min were almost overlapped, with the σ_f of ~0.6 MPa and λ_f of ~4.8. This indicated

the polymerization and crosslinking process triggered by mechanoradicals nearly completed at v = 30 mm/min, during which the loading time of gel from yield stretch ratio to fracture stretch ratio of was about 2 min.

4.3.2 Single edge notched test

We then performed the single edge notched tests to systematically exhibit how mechanoradical polymerization around the crack tip improved the ability of DN gels to resist crack initiation (**Figure 4.8**). DN gels are a class of tough hydrogels with the relatively large dissipation length ξ about 0.01-1 mm[2,17]. When the crack length c exceeds this dissipative length ξ, the stretchability of notched DN gels decreases a lot compared with unnotched DN gels. As demonstrated in the uniaxial tensile test, an unnotched dumbbell-shaped DN-H_2O gel could be stretched to 10 times its original. However, when an initial crack (crack length c = 1 mm) was introduced to the DN-H_2O gel, the catastrophic failure occurred early with $\lambda_f \sim 2.3$, close to but ahead of the yield point of the unnotched sample (**Figure 4.8b**, v = 10 mm/min). With the cut length further increased from 1 mm to 5 mm, the fracture stretch ratio decreased to 1.8 and fracture stress decreased to 0.08 MPa (**Figure 4.8d, e**). **Figure 4.9a** shows the fracture process of notched DN-H_2O (c = 1 mm) with the assistance of the birefringence observation. At $\lambda \sim 1.7$, a small yet distinguishable damage zone appeared in the crack tip. As stretch continued, crack tip kept blunting with the increase in damage zone up to the crack initiation at $\lambda \sim 2.3$. To better understand the crack initiation process of notched DN gels, the field approach is applied in the following qualitatively discussion[1,2]. We consider the crack initiation is controlled by the true stress directly

ahead of the crack tip σ_{tip}. Crack initiation occurs at the condition $\sigma_{tip} = \sigma_{f,T,}$ where $\sigma_{f,T}$ is the true fracture stress. For DN-H_2O gel with a crack of c = 1 mm, σ_{tip} exceeded $\sigma_{f,T}$ before the stress in the gel bulk reached the yield stress, resulting in the crack initiation ahead of the yield strain. Such crack initiation process of DN-H_2O was independent of the loading rate (**Figure 4.11**).

By contrast, DN-DAC gel with the same crack at the same loading rate (c = 1 mm, *v* = 10 mm/min) fractured at the $\lambda \sim 4.2$ (**Figure 4.8c**). This fracture stretch ratio of notched DN-DAC was just slightly smaller than that of unnotched DN-DAC gel and was much larger than that of notched DN- H_2O gel. As shown in **Figure 4.9b**, at $\lambda \sim$ 2.3, the crack initiation didn't happen in notched DN-DAC gels. The crack tip continued to blunt and showed a wider damage zone near the crack tip, indicated by the whitening region in the birefringence image. With the increase of λ, the necked region gradually developed into the whole notched DN-DAC gel as like the unnotched gel. This clearly implies the $\sigma_{f,T}$ of the crack tip was improved so that even the stress in gel bulk reached the yield stress, σ_{tip} was still smaller than the improved $\sigma_{f,T}$. After the completion of necking, the stress in the gel bulk restarted to increase, resulting in the increase of σ_{tip}. The crack initiation finally occurred when the σ_{tip} exceeded the improved $\sigma_{f,T}$. For DN-DAC gel with the crack length c = 2 mm (**Figure 4.8c-e**), the crack initiation also occurred after the completion of necking, with the fracture stretch ratio ~ 3.8. However, if crack length was increased from c = 2 mm to c = 5 mm, the crack initiation was ahead of the necking strain, with the fracture stretch ratio remarkably decreased from 3.8 to 2.0. This means the enhanced crack tip could not

afford the necking of the gel bulk, which should be attribute to the amplitude of the stress concentration. Even so, this fracture stretch ratio of DN-DAC was still slightly larger compared to DN-H_2O.

Considering the fact that notched DN gel only containing monomer DAC yet no crosslinker MBA showed no enhanced crack resistance (**Figure 4.13**), it is believed that the radicals generated near the crack tip triggered the formation of a new network, which enhanced the crack tip and delayed the crack initiation. Since the pre-existing first network is negative charged polyelectrolyte PAMPS and second network is neutral polymer PAAm while the expected newly-formed network poly DAC is positive charged, we can use anionic dye methyl blue to mark the region where poly DAC network is formed. The notched DN-DAC gel (c = 1 mm) was loaded to different maximum stretch ratio and then unloaded for the following dying. As shown in **Figure 4.10**, at the small stretch ratio of 1.7, the region near crack tip had appeared blue, indicating the formation of poly DAC network. With the increase of stretch ratio, the blue area increased and then expanded to the whole gauge of the gel, which is highly consistent with the birefringence observation.

Since mechanoradical polymerization and crosslinking process is relatively slow process, such enhancement effect shows strong rat-dependence. As shown in **Figure 4.11**, the delay of crack initiation only worked at the slow loading rate (v = 10, 30 mm/min). At the fast loading rate (v = 50, 100, 300 mm/min), the fracture stretch ratio of notched ND-DAC decreased to the same level of notched DN-H_2O. To prevent the crack initiating before necking, there exists a critical loading rate v_c which gives enough

time to form an effective network in the crack tip to support the necking in the gel bulk. If we define the stretch ratio that crack tip starts to neck and generates mechanoradicals as the λ_{tip-y} and define stretch ratio that crack initiates without polymerization as the λ_{tip-f}, the critical loading rate v_c can be expressed in the following equation:

$$v_c = \frac{(\lambda_{tip-f} - \lambda_{tip-y}) \times L}{t_p} \qquad (1)$$

Where L is the gauge length of the gel (L = 20 mm in this case) and t_p is the polymerization time to form an effective network. From the uniaxial tensile test, t_p is estimated about 0.5 min to 2 min. And from the birefringence observation of fracture process of notched sample, λ_{tip-y} is estimated about 1.7 and λ_{tip-f} is 2.3. Thus, the estimated v_c is about 6 mm/min - 24 mm/min, which is in the same order of the experiment value of 30 mm/min from **Figure 4.11**.

To further increase the fracture stretch ratio of notched DN-DAC gel, programmed tensile procedure was adopted. As shown in **Figure 4.12**, the notched DN-DAC gel (c = 1 mm) was first stretched to $\lambda = 2.3$ at $v = 10$ mm/min to induce the network formation in the crack tip. Then the loading rate was increased to 300 mm/min to avoid the network formation in the gel bulk during the deformation. By this way, the fracture stretch ratio of notched DN-DAC was increased to ~ 6.5.

We then have a short conclusion on the single edge tensile test from the view of fracture toughness. For DN-H_2O gel, the fracture toughness in the crack tip Γ_{tip} is same with the toughness in the gel bulk Γ_{bulk} at all loading rates. For DN-DAC gel, at the fast loading rate, Γ_{tip}^{fast} still can be considered equal to Γ_{bulk}^{fast}. However, at the slow loading rate, due to the mechanoradical polymerization, Γ_{tip}^{slow} is larger than Γ_{tip}^{fast} and thus

larger than Γ_{bulk}^{slow}.

4.3.3 Pure shear test and trouser tearing test

Then we demonstrate how this unique rate-dependent enhancement in the crack tip influences the crack propagation behavior. Pure shear tests, which have large sample length and thus allow the observation of the crack propagations[1,2], were first performed on the notched DN-H_2O and DN-DAC gels (**Figure 4.14a**). Similar to the single edge notched test, DN-DAC gel with a large crack showed slightly larger critical stretch ratio than DN-H_2O gel only at the slow loading rate of v = 10 mm/min (**Figure 4.14b, c**). However, the crack propagation mode was totally different. For notched DN-H_2O, the crack initiation started at the stretch ratio $\lambda \sim 2.1$, with a triangular damage zone appeared in the crack tip (**Figure 4.14d**). After that, the crack propagated in a slow speed about 0.01 m/s (**Figure 4.15**). For notched DN-DAC gel, the crack initiation didn't occur at the $\lambda \sim 2.1$. With the increase of stretch ratio to ~2.5, DN-DAC gel had a larger blunting tip (**Figure 4.14e**) and then underwent a catastrophic failure in a fast speed about 1 m/s (**Figure 4.15**). The catastrophic failure of the DN-DAC was induced by the overstretch of the bulk DN-DAC[24]. The increase of Γ_{tip} resulted in the increase of critical stretch ratio. This made the energy release rate in the gel bulk G_{bulk} much exceeded the $\Gamma_{bulk,}$ resulting in the fast crack propagation after crack initiation.

Trouser tearing tests were then performed (**Figure 4.16a**). The most characteristic of the trouser tearing test is that, with the tensile of the legs, the new crack tip constantly generates whereas the rest gel bulk are free of loading[1,25]. For DN-H_2O gel, the crack propagated in a steady state mode at all loading rates (**Figure 4.16b**) and a smooth

surface was left after fracture (**Figure 4.16e**). The average fracture toughness Γ_{av} was decreased from 1100 J/m^2 to 750 J/m^2 with the decrease of v from 300 mm to 10 mm/min, showing a weak dependence on the loading rate due to the decrease of the damage zone (**Figure 4.16d**). For DN-DAC gel, at the fast-loading rate (30 mm/min – 300 mm/min), the crack propagated in a weak stick-slip instability mode and Γ_{av} was decreased from ~750 J/m^2 to ~250 J/m^2 with the decrease of loading rate (**Figure 4.16c, d**). However, with the loading rate further decreased to 10 mm/min, which gave enough time to form a strong network to enhance the crack tip, the crack propagated in a much-intensified stick-slip mode and a rough surface was left after fracture (**Figure 4.16f**). Γ_{av} of DN-DAC at 10 mm/min is higher than that of DN-DAC at the fast-loading rate, and also higher than that of DN-H_2O at the same loading rate.

4.3.4 The generality of the strategy

The crack enhancement via mechanoradical polymerization is common for diverse monomers. This was shown by a set of experiments in which the DN gels were fed with various monomers (2-acrylamido-2-methyl-1-propanesulfonic acid sodium (NaAMPS), acrylamide (AAm), N-isopropyl acrylamide (NIPAm), 2.0 M) and a MBA crosslinker (0.15 M). The previously demonstrated DAC is a representative of cationic monomer. Here, NaAMPS is a representative of anionic monomer while AAm and NIPAm are representatives of neutral monomer. As shown in **Figure 4.17**, under the single edge notched test (v = 10 mm/min), all DN gels showed the remarkable increase of fracture stretch ratio compared with the DN-H_2O at the slow loading rate, indicating the enhancement of the crack tip.

4.4 Conclusion

We demonstrated the rate-dependent enhanced crack resistance of DN gels via mechanoradical polymerization. At the slow loading rate, the crack tip enhancement via mechanoradical polymerization improved the stretchability of notched sample under the single edge notched test, induced the fast crack propagation under the pure shear test and the stick-slip behavior under the tearing test. Two-section rate-dependent tensile behavior of the gel was also demonstrated. Though it is not investigated due to the limitation of the tensile machine in the glove box, the mechanical behavior is expected to be independent of the of loading rate at the extreme slow or fast loading. This method holds great potential to on-demand adjust the material's rate-dependent behavior by controlling the kinetics of polymerization and crosslinking, e.g., controlling the mechanoradical concentration in the gel or controlling the monomer species and concentration.

4.5 References

1. Long, R.; Hui, C. Fracture toughness of hydrogels: measurement and interpretation. *Soft Matter* **2016**, *12*, 8069-8086.
2. Long, R.; Hui, C.; Gong, J. P.; Bouchbinder, E. The fracture of highly deformable soft materials: A tale of two length scales. *Annu. Rev. Condens. Matter Phys.* **2021**, *12*, 71–94.
3. Creton, C.; Ciccotti, M. Fracture and adhesion of soft materials: A review. *Rep. Prog. Phys.* **2016**, *79*, 046601.
4. Chen, C., Wang, Z., Suo, Z. Flaw sensitivity of highly stretchable materials. *Extreme Mech. Lett.* **2017**, *10*, 50-57.
5. Persson, B. N. J., Albohr, O., Heinrich, G., Ueba, H. Crack propagation in rubber-like materials. *J. Phys.: Condens. Matter* **2005**, *17*, R1071.
6. Ducrot, E., Chen, Y., Bulters, M., Sijbesma, R. P., Creton, C. Toughening elastomers with sacrificial bonds and watching them break. *Science* **2014**, *344*, 186-189.
7. Creton, C. 50th anniversary perspective: Networks and gels: soft but dynamic and tough. *Macromolecules* **2017**, *50*, 8297−8316.
8. Zhao, X., Chen, X., Yuk, H., Lin, S., Liu, X., Parada, G. Soft materials by design: unconventional polymer networks give extreme properties. *Chem. Rev.* **2021**, *121*, 4309-4372.
9. Kim, J., Zhang, G., Suo, Z. Fracture, fatigue, and friction of polymers in which entanglements greatly outnumber cross-links. *Science* **2021**, *374*, 212-216.

10. Gong, J. P.; Katsuyama, Y.; Kurokawa, T.; Osada, Y. Double network hydrogels with extremely high mechanical strength. *Adv. Mater.* **2003**, *15*, 1155−1158.
11. Sun, J.Y., Zhao, X., Illeperuma, W.R., Chaudhuri, O., Oh, K.H., Mooney, D.J., Vlassak, J.J. and Suo, Z. Highly stretchable and tough hydrogels. *Nature*, **2012**, 489, 133-136.
12. Sun, T.L., Kurokawa, T., Kuroda, S., Ihsan, A.B., Akasaki, T., Sato, K., Haque, M.D., Nakajima, T. and Gong, J.P. Physical hydrogels composed of polyampholytes demonstrate high toughness and viscoelasticity. *Nat. Mater.* **2013**, 12, 932-937.
13. Zheng, S. Y.; Ding, H. Y.; Qian, J.; Yin, J.; Wu, Z. L.; Song, S. Y.; Zheng, Q. Metal-coordination complexes mediated physical hydrogels with high toughness, stick−slip tearing behavior, and good processability. *Macromolecules* **2016**, 49, 9637-9646.
14. Mredha, M.T.I., Guo, Y.Z., Nonoyama, T., Nakajima, T., Kurokawa, T., Gong, J.P. A facile method to fabricate anisotropic hydrogels with perfectly aligned hierarchical fibrous structures. *Adv. Mater.* **2018**, *30*, 1704937.
15. Hua, M., Wu, S., Ma, Y. et al. Strong tough hydrogels via the synergy of freeze-casting and salting out. *Nature* **2021**, *590*, 594–599.
16. Liu, C., Morimoto, N., Jiang, L., Kawahara, S., Noritomi, T., Yokoyama, H., Mayumi, K., Ito, K. Tough hydrogels with rapid self-reinforcement. *Science* **2021**, *372*, 1078-1081.

17. Liang, S., Wu, Z. L., Hu, J., Kurokawa, T., Yu, Q. M., Gong, J. P. Direct observation on the surface fracture of ultrathin film double-network hydrogels. *Macromolecules* **2011**, *44*, 3016-3020.

18. Matsuda, T.; Kawakami, R.; Nakajima, T.; Gong, J. P. Crack tip field of a double-network gel: visualization of covalent bond scission through mechanoradical polymerization. *Macromolecules* **2020**, *53*, 8787−8795.

19. Zapp, C., Obarska-Kosinska, A., Rennekamp, B. Kurth, M., Hudson, D. M., Mercadante, D., Barayeu, U., Dick, T. P., Denysenkov, V., Prisner, T., Bennati, M., Daday, C., Kappl, R., Grater, F. Mechanoradicals in tensed tendon collagen as a source of oxidative stress. *Nat. Comm.* **2020**, *11***,** 2315.

20. Sakai, H.; Sumi, T.; Aoki, D.; Goseki, R.; Otsuka, H. Thermally stable radical-type mechanochromic polymers based on difluorenylsuccinonitrile. *ACS Macro Lett.* **2018**, *7*, 1359–1363.

21. Zheng. Y.; Matsuda. T.; Nakajima. T.; Cui. W.; Zhang. Y.; Hui. C.; Kurokawa. T.; Gong. J. P. How chain dynamics affects crack initiation in double-network gels. *Proc. Natl. Acad. Sci.* **2021**, *118*, e2111880118.

22. Furukawa, H.; Kuwabara, R.; Tanaka. Y.; Kurokawa. T.; Na. Y.; Osada, Y.; Gong, J. P. Tear velocity dependence of high-strength double network gels in comparison with fast and slow relaxation modes observed by scanning microscopic light scattering. *Macromolecules* **2008**, *41*, 7173-7178.

23. Batch, G. L., Macosko, C. W. Kinetic model for crosslinking free radical polymerization including diffusion limitations. *J. Appl. Poly. Sci.* **1992**, *44*, 1711-1729.

24. Zhang, Y., Fukao, K., Matsuda, T., Nakajima, T., Tsunoda, K., Kurokawa, T., Gong, J. P. Unique crack propagation of double network hydrogels under high stretch. *Extreme Mech. Lett*. **2022**, *51*, 101588.

25. Liang, S.; Hu, J.; Wu. Z. L.; Kurokawa. T.; Gong, J. P. Toughness enhancement and stick−slip tearing of double-network hydrogels in poly(ethylene glycol) solution. *Macromolecules* **2012**, *45*, 4758−4763.

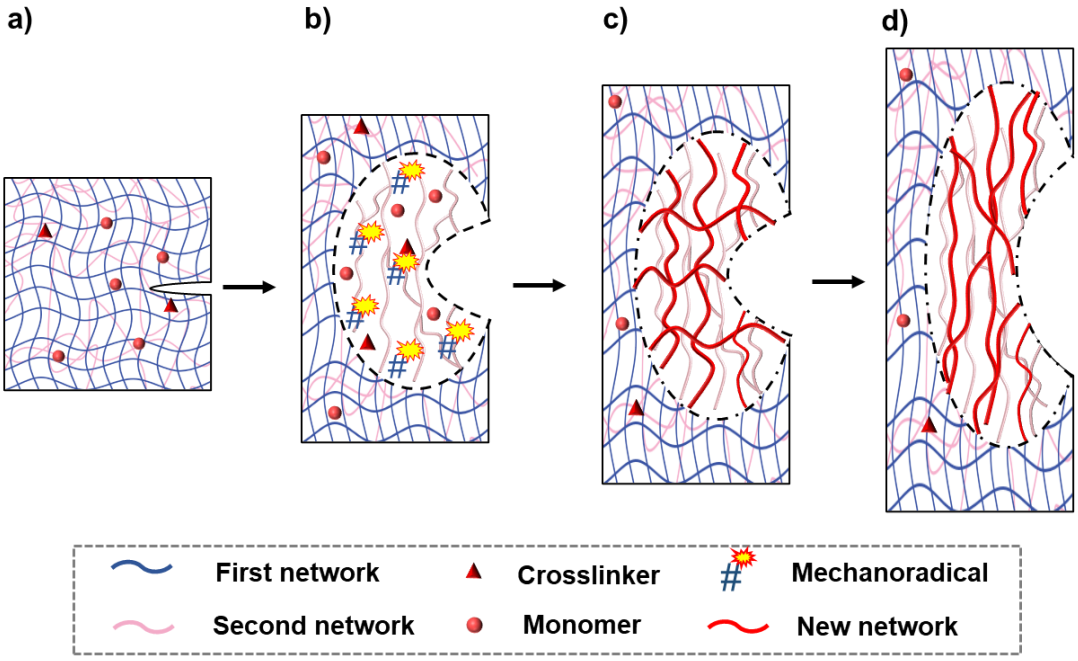

Figure 4.1. Conceptual Scheme of the crack resistance enhancement via mechanoradical polymerization in double network (DN) hydrogels. a) A notched DN gel fed with monomers and crosslinkers. b) Upon deformation, stress concentrates in the crack tip, resulting in the early bond rupture in first network and mechanoradical generation. c) Mechanoradicals trigger the formation of a new network in the crack tip. d) The notched DN gel with the newly formed network can be subjected to larger deformation.

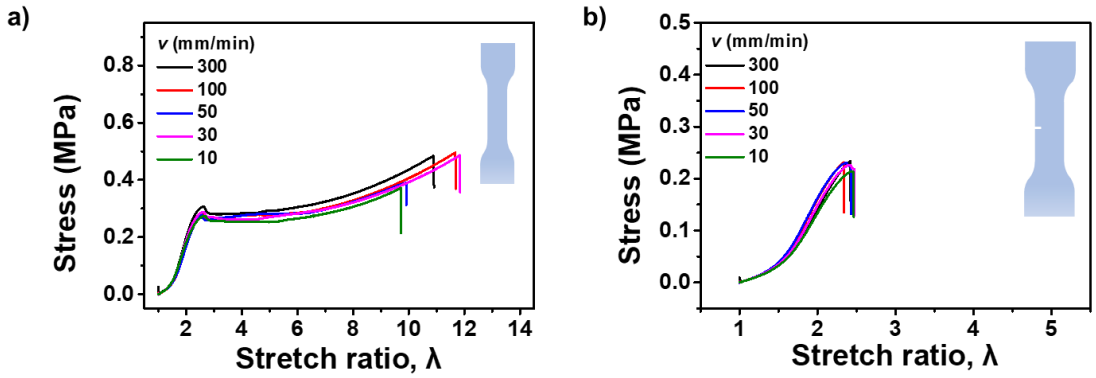

Figure 4.2. Stress-stretch ratio curves of DN-DAC gels when performed the tensile test (a) and single edge notched test (b) in air at different loading rates.

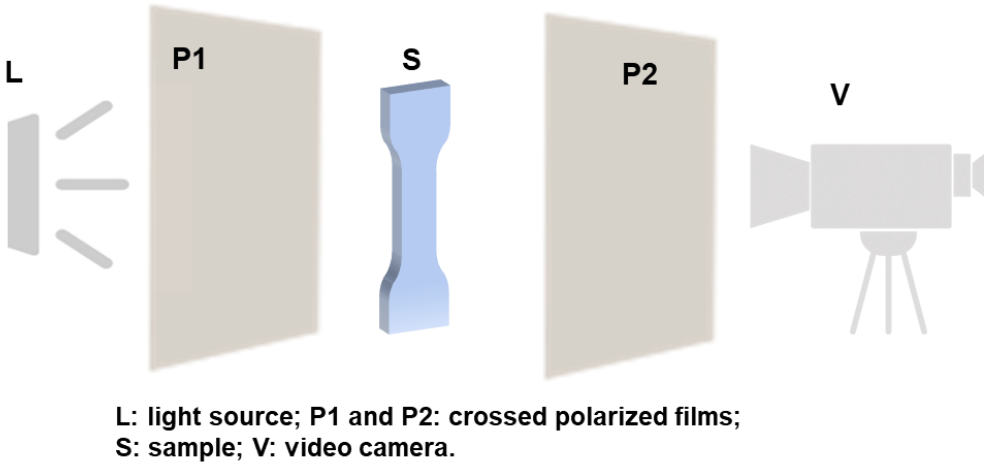

Figure 4.3. Schematic of birefringence observation in the tensile tests and following single edge notched tests and pure shear tests.

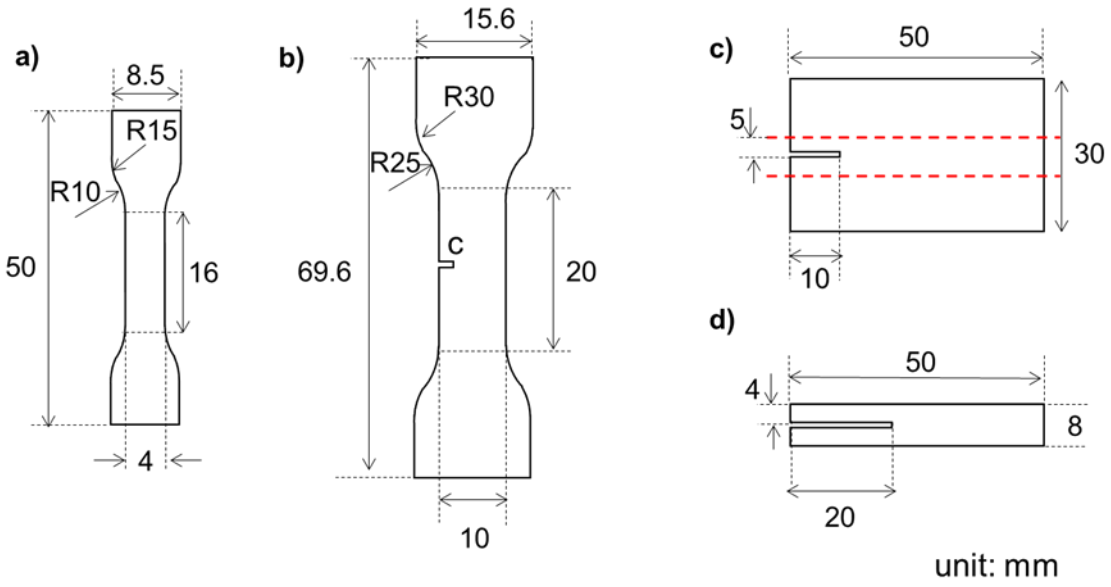

Figure 4.4. The geometries of the cut gels used for tensile test (a), single edge notched test (b), pure shear test (c) and tearing test (d). In single edge notched tests, crack length c is varied from 0 mm to 5 mm. In pure shear test, the samples are fixed along the red dashed lines.

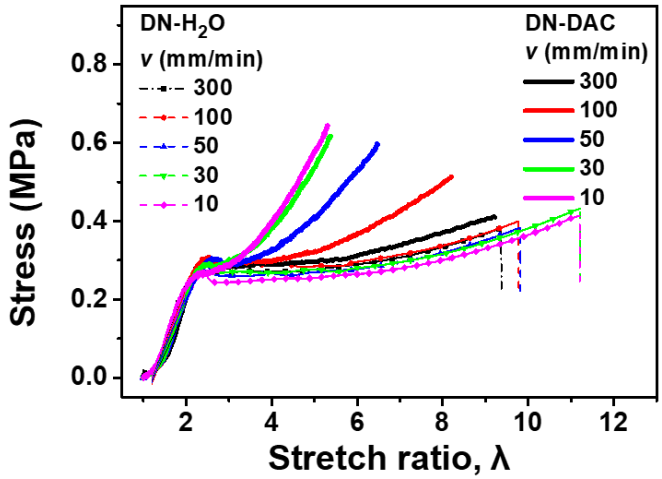

Figure 4.5. Stress-stretch ratio curves of dumbbell-shaped DN-H_2O and DN-DAC at the different loading rate *v* in the argon glove box.

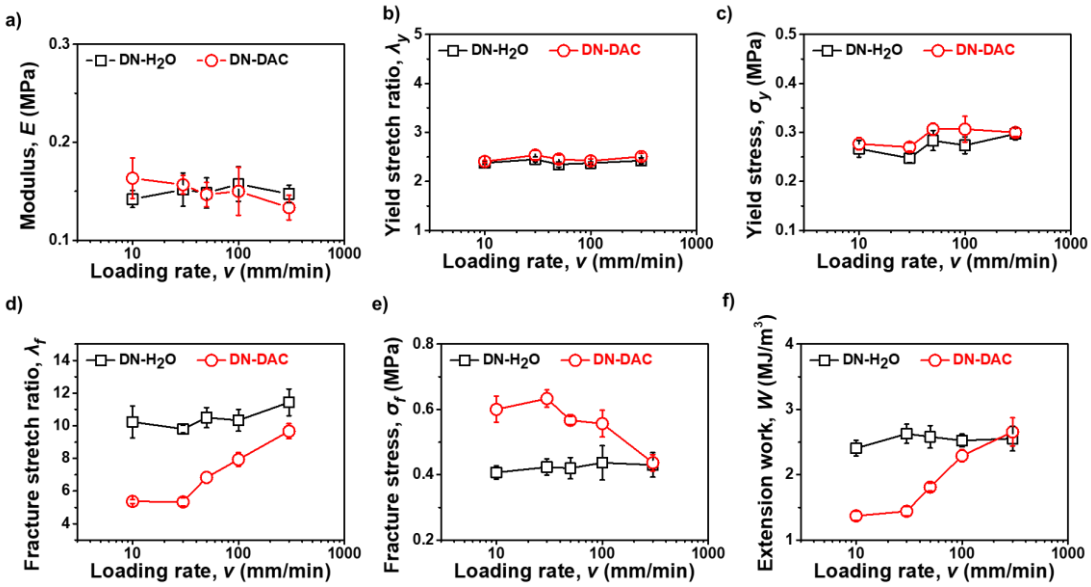

Figure 4.6. Statistics of mechanical properties of DN-H_2O and DN-DAC gels when performed tensile tests in the argon glove box at the different loading rates.

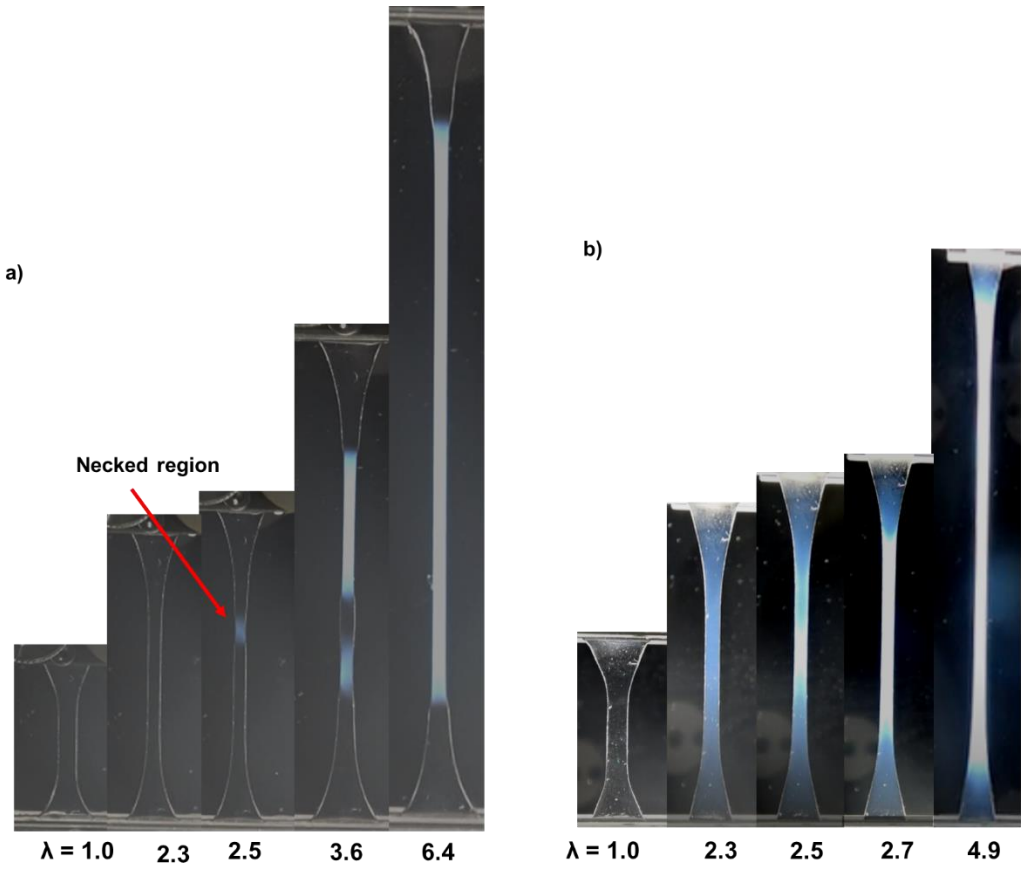

Figure 4.7. Birefringence images of and DN-H_2O and DN-DAC gels when performed the tensile test at the glove box (v = 10 mm/min) at the various stretch ratio λ.

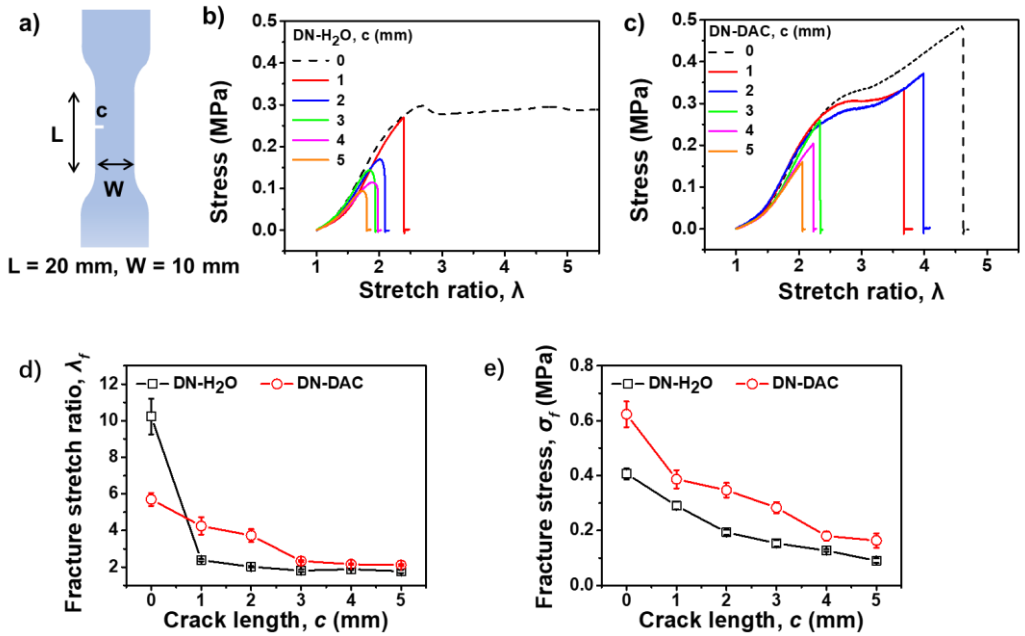

Figure 4.8. Rate-dependent mechanical behavior of DN-H_2O and DN-DAC gels under the single edge notched test in the glove box. a) Geometry of the sample for single edge notched test. b, c) Stress-stretch ratio curves of DN-H_2O (b) and DN-DAC (c) gels with different initial crack length c (loading rate v = 10 mm/min). d, e) Influence of the crack length on the fracture stretch ratio (d) and fracture stress (e) of DN-H_2O and DN-DAC gels. The loading rate is 10 mm/min.

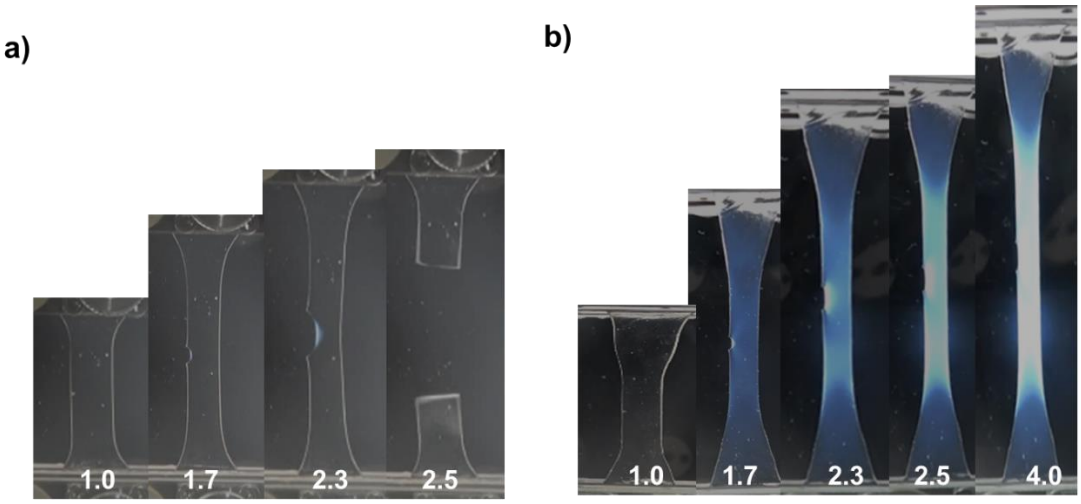

Figure 4.9. Birefringence images of notched DN-H_2O (a) and DN-DAC (b) gels (c = 1 mm, *v* = 10 mm/min) at the different stretch ratio (shown in the bottom of images) at the glove box.

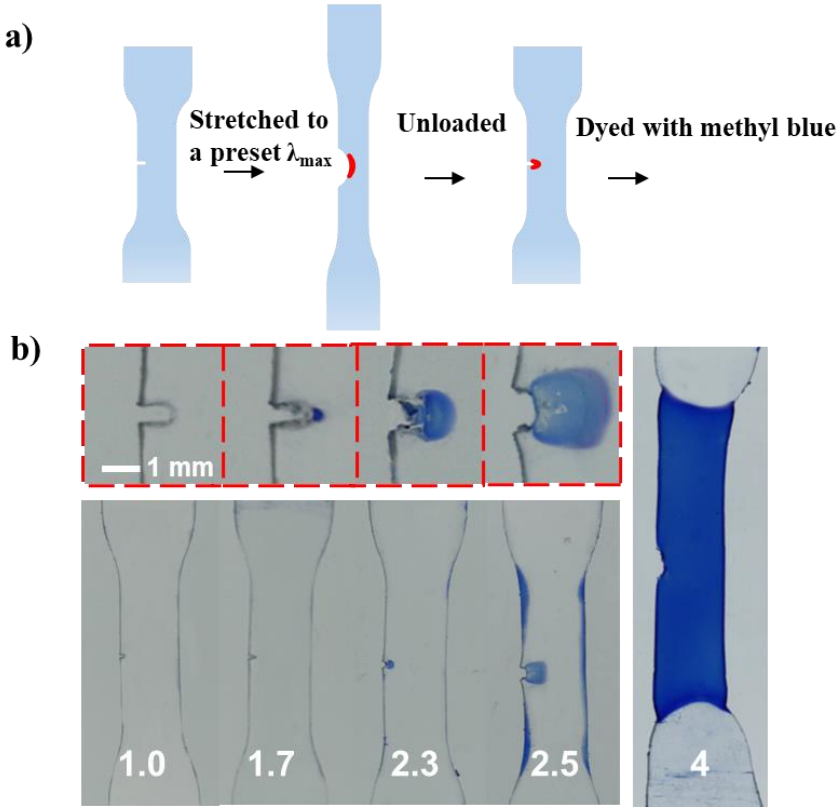

Figure 4.10. a) Illustration of dyeing the damage zone of the notched DN-DAC gels after stretching to different preset tensile stretch ratio. b) Photo images of notched DN-DAC gels (c = 1 mm, *v* = 10 mm/min) after stretched to the different preset strain, unloaded, then dyed with methyl blue. Enlarged images of the crack tip are shown in the red dashed line.

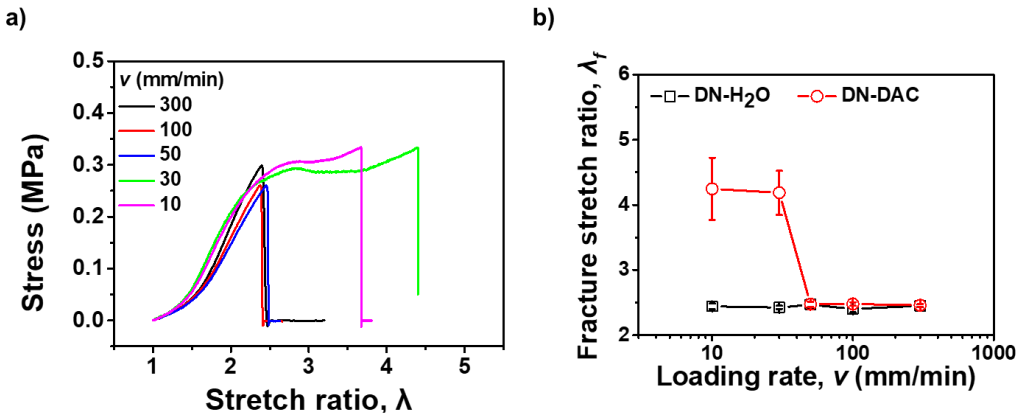

Figure 4.11. a) Tensile stress-strain curves of notched DN-DAC (c = 1 mm) gels at the different loading rate. b) Fracture stretch ratio of notched DN-H_2O and DN-DAC (c = 1 mm) as a function of loading rate.

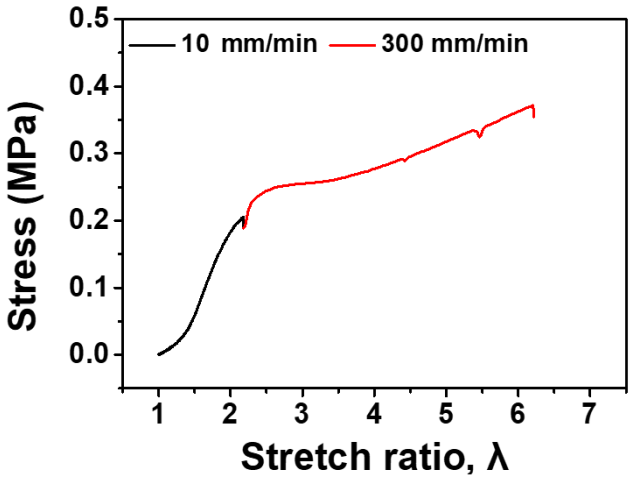

Figure 4. 12. Stress-stretch ratio curve of notched DN-DAC (c = 1 mm) when performed programed tensile procedure in the glove box.

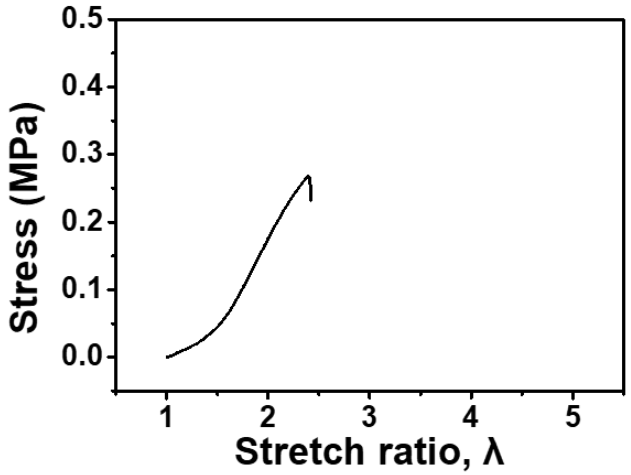

Figure 4.13. Stress-stretch ratio curve of notched DN gels containing monomer DAC yet no crosslinker MBA (c = 1 mm, v = 10 mm/min) when performed single edge notched test in the glove box.

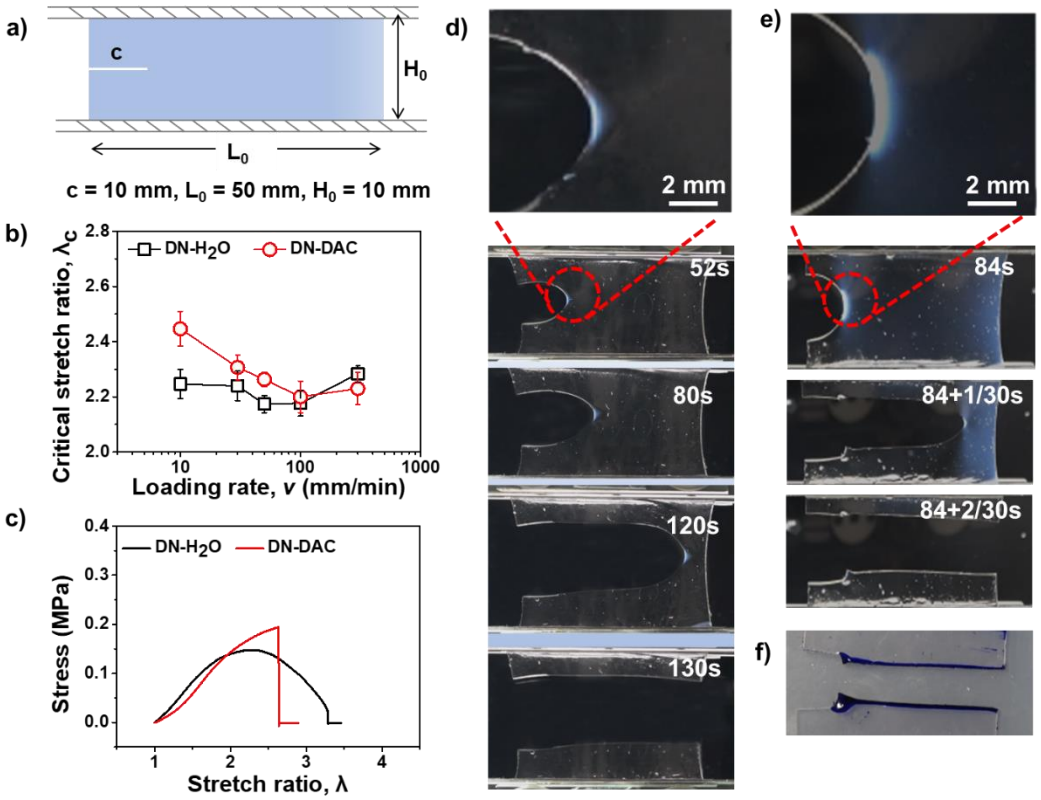

Figure 4.14. Pure shear test of DN-H_2O and DN-DAC gels. a) Geometry of the sample for pure shear test. b) Critical stretch ratio as a function of the loading rate. c) stress-stretch ratio curves of DN-H_2O and DN-DAC at the loading rate of v = 10 mm/min. d,e) Representative birefringence images showing the crack propagation behavior of DN-H_2O (d) and DN-DAC (e). The crack tip at the onset of crack propagation (in red dashed line) is enlarged. f) Photo images of fractured DN-DAC gel after dyeing.

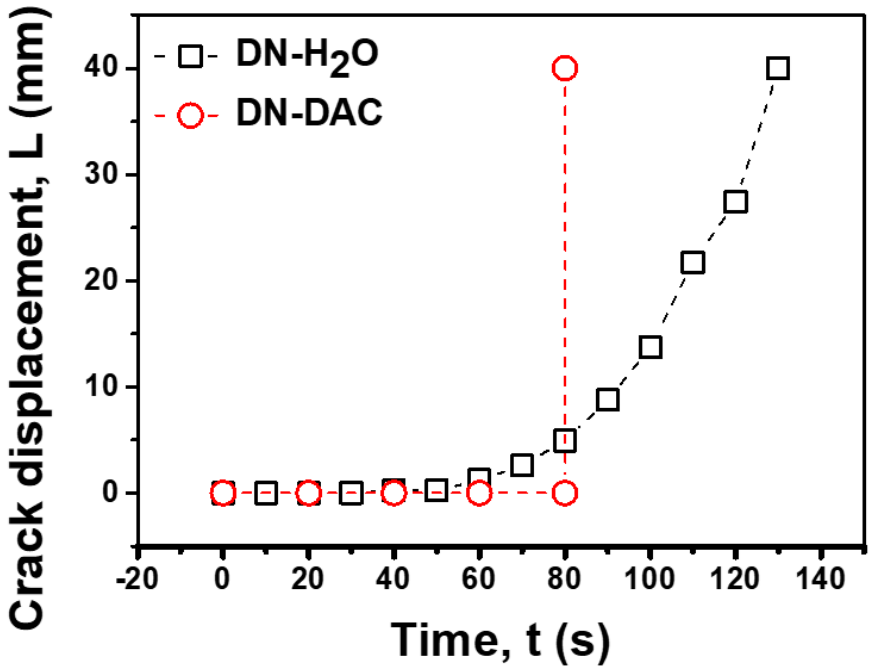

Figure 4.15. Crack displacement-time curves of DN-H_2O and DN-DAC gels under the pure shear test in the glove box. The loading rate is 10 mm/min.

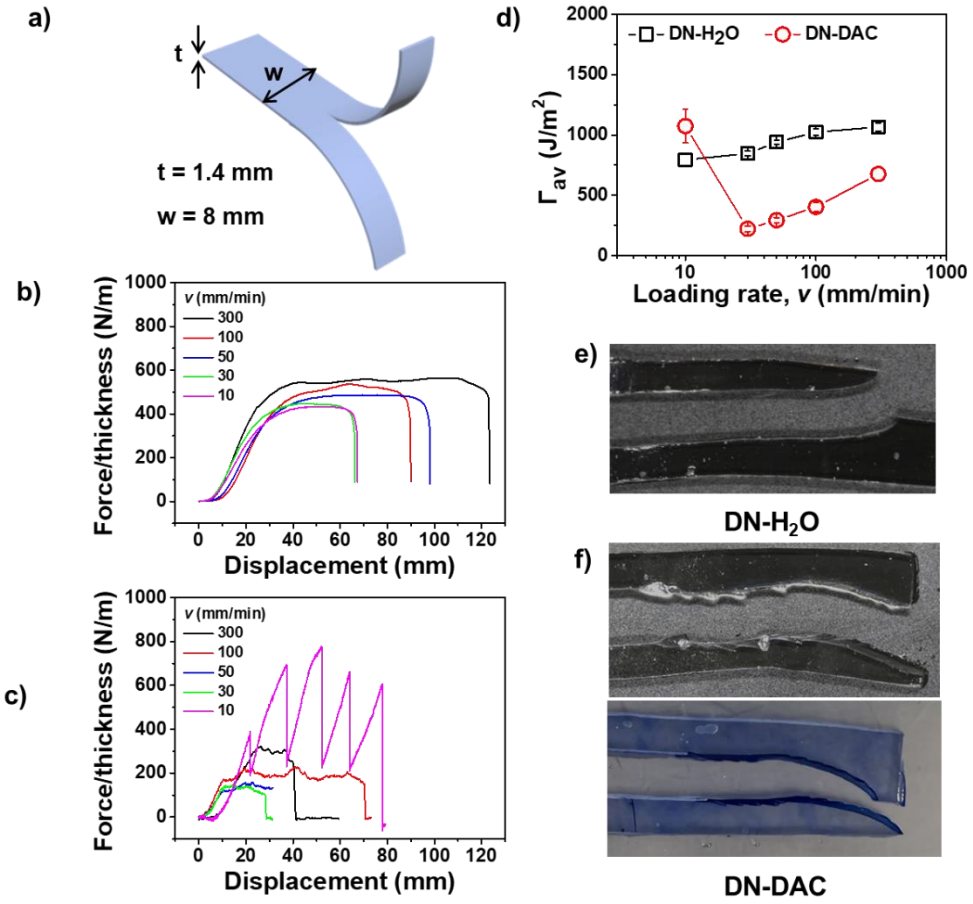

Figure 4.16. Trouser tearing test of DN-H_2O and DN-DAC gels. a) Geometry of the sample for trouser tearing test. b,c) Normalized tearing force-displacement curves of DN-H_2O (b) and DN-DAC (c) at different loading rates. d) Averaged fracture energy as a function of loading rate. e) Photo images of fractured DN-H_2O. f) Photo images of fractured DN-DAC gels before (top) and after (bottom) dyeing.

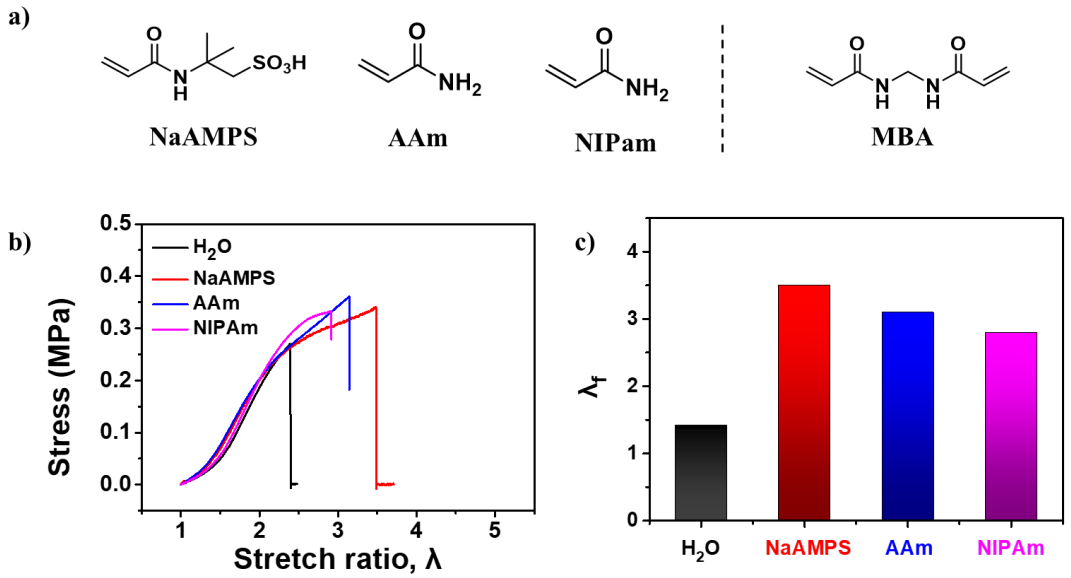

Figure 4.17. a) Chemical structure of different monomers with a same crosslinker MBA. b,c) Stress-stretch ratio curves of notched DN gels fed with different monomers under the single edge notched test in the glove box and corresponding fracture stretch ratio λ_f as a function of monomer varieties.

Table 4.1. Shrinkage ratio in length, *f*, of DN gels when immersed into different monomer solutions with the presence of crosslinker MBA. Shrinkage ratio in length was calculated by dividing the diameter of the gel in the monomer solutions and in water.

Monomer	DAC	NaAMPS	NIPAm	AAm
f	0.95 ± 0.01	0.92 ± 0.02	0.93 ± 0.01	0.98 ± 0.01

Chapter 5: General Conclusion and Outlook

Chemically reactive mechanoradical generated by the bond rupture is a promising tool to design mechano-responsive polymer materials. This dissertation describes how to improve the mechanoradical concentration in the DN gels and demonstrates two examples of introducing new functions to the DN gels with the increased concentration of mechanoradicals. The main conclusions were as follows:

At first, we demonstrate the polymer strand density and the ratio of broken strands are the two factors that directly determine the mechanoradical concentration. Incorporating the weak azoalkane crosslinker into the first network of DN gels is an effective way to significantly increase the ratio of broken strands. We found in the azoalkane-crosslinked DN gels, the concentration of mechanoradicals can reach a maximum of ~220 μM, which is 5 times that of the traditional crosslinker. Employing a mixture of traditional crosslinker and azoalkane crosslinkers also results in an excellent performance in generating mechanoradicals.

Then, we demonstrate that azo-crosslinked DN gels can show near full plasticity via mechanoradical polymerization in the deformed gels. The mechanoradical-trigged new network in the deformed gels counterbalances the retraction of the original network and maintains the force-induced deformation permanently. With this plasticity, we successfully regulate the sheet-shaped gels into various three-dimensional shapes at ambient temperature by applying blowing forming and drawing forming.

We also successfully improved the crack resistance of azo-crosslinked DN gels via mechanoradical polymerization in the crack tip. The mechanoradical-triggered new

network in the crack tip enhances the crack tip, which improves the stretchability of notched DN gels and changes the crack propagation behavior. Since the relatively slow polymerization process, such enhancement only works at the slow loading rate. We also demonstrate the unique two-section rate-dependent tensile behavior that mechanical properties before the yield strain is independent of the tensile rate while that after the yield strain is strongly affected by the tensile rate.

Here, we must emphasize that a large number of mechanoradicals in DN gels only are generated in the necked region after reaching the yield strain because extensive bond rupture of the first network only occurs in the necked region. It is crucial for understanding the mechanical behavior of DN gels when fed with monomers and crosslinkers.

In summary, this work shows a new method to improve the mechanoradical concentration in the DN gels and provides a new sight into the application of mechanoradicals. Besides the mechanoradical polymerization, the increased concentration of mechanoradicals should make it easier to trigger other radical-involved organic and inorganic reactions and thus to impart more mechano-responsive functions to the materials. We believe that this work will promote the application of DN gels in more fields and should expand the research scope in the mechanochemistry.

List of Publications

1. Zhi Jian Wang, Julong Jiang, Qifeng Mu, Satoshi Maeda, Tasuku Nakajima, Jian Ping Gong, Azo-Crosslinked double-Network Hydrogels Enabling Highly Efficient Mechanoradical Generation, Journal of the American Chemical Society, 2022, 144, 7, 3154-3161.
2. Zhi Jian Wang, Tasuku Nakajima, Jian Ping Gong, Hydrogel Morphogenesis Induced by Force-Controlled Growth, submitted.
3. Zhi Jian Wang, Xueyu Li, Tasuku Nakajima, Jian Ping Gong, Enhanced Crack Resistance of Double Network Hydrogels via Mechanoradical Polymerization in the Crack Tip, in preparation.

Acknowledgement

This dissertation represents the culmination of three years (2019-2022) at the Laboratory of Soft and Wet Matter (LSW), Graduate School of Life Science, Hokkaido University, Japan. I am incredibly grateful to all those people who contributed to this work and provided varying degrees of assistance, encouragement, and guidance to me.

I wish to first express my appreciation and respect to my supervisors Professor Jian Ping Gong and Associated Professor Tasuku Nakajima. They have abundant experience and wide knowledge and are supportive to give me a lot of scientific and insightful suggestions on the experiment design, data analysis, and paper writing. Through discussion with them, I could have a deep understanding of the research. They are also kind to give me the freedom to do things in my own order, making me free of anxiety and pressure.

I also must thank my master's degree supervisor, Zi Liang Wu, an old member of LSW. He gave me the confidence to pursue a doctoral degree and recommended me to Professor Gong so that I could get a position in the LSW. Without him, I would not have chance to write this acknowledgment.

I also would like to thank Professor Satoshi Maeda and Assistant Professor Julong Jiang in the department of chemistry who performed excellent chemical calculations on the mechanophores. I also thank Professor Yi Cao and Yiran Li at Nanjing University who shared the results of single-molecule force spectroscopy of the azoalkane. They are the key collaborators in my research and improve the work to a higher level.

Then, I would like to thank all the excellent members in our group. It is a great

pleasure to work and live with them. They, Associate Professor Takayuki Nonoyama, Assistant Professor Xueyu Li, technical staff Yukiko Hane and Yoshinori Katsuyama, secretaries Eiko Hasegawa and Saeko Iseya, students Qifeng Mu, Ryuji Kiyama…all supported me a lot during the experiment and daily life.

I thank the scholarship support from the Ministry of Education, Culture, Sports, Science, and Technology (MEXT) in Japan.

Finally, I would like to express my appreciation to my father, my mother, my sister, my wife and my son for their enduring support and love for me during my doctoral work.

Zhi Jian Wang

Division of Soft Matter

Graduate School of Life Science

Hokkaido University, Japan

June 2022